2010

Regulation of Sealing Ring Formation by L-plastin and Cortactin in Osteoclasts

Tao Ma
Dental School, University of Maryland

Kavitha Sadashivalah
Dental School, University of Maryland

Nandakumar Madayiputhiya
University of Nebraska-Lincoln

Meenakshi A. Chellaia
Dental School, University of Maryland, mchellaiah@umaryland.edu

ADDITIONS AND CORRECTIONS

This paper is available online at www.jbc.org

THE JOURNAL OF BIOLOGICAL CHEMISTRY VOL. 286, NO. 14, p. 12812, April 8, 2011

VOLUME 285 (2010) PAGES 29911–29924
DOI 10.1074/jbc.A109.099697

Regulation of sealing ring formation by L-plastin and cortactin in osteoclasts.

Tao Ma, Kavitha Sadashivaiah, Nandakumar Madayiputhiya, and Meenakshi A. Chellaiah

The revised author list is shown above. Dr. Madayiputhiya's affiliation is the Nebraska Redox Biology Center, University of Nebraska-Lincoln, Lincoln, Nebraska 68588.

THE JOURNAL OF BIOLOGICAL CHEMISTRY VOL. 285, NO. 39, pp. 29911–29924, September 24, 2010

Regulation of Sealing Ring Formation by L-plastin and Cortactin in Osteoclasts*[S]

Received for publication, December 28, 2009, and in revised form, June 11, 2010 Published, JBC Papers in Press, July 22, 2010, DOI 10.1074/jbc.M109.099697

Tao Ma, Kavitha Sadashivaiah, and Meenakshi A. Chellaiah[1]

From the Department of Oncology and Diagnostic Sciences, Dental School, University of Maryland, Baltimore, Maryland 21201

The aim of this study is to identify the exact mechanism(s) by which cytoskeletal structures are modulated during bone resorption. In this study, we have shown the possible role of different actin-binding and signaling proteins in the regulation of sealing ring formation. Our analyses have demonstrated a significant increase in cortactin and a corresponding decrease in L-plastin protein levels in osteoclasts subjected to bone resorption for 18 h in the presence of RANKL, M-CSF, and native bone particles. Time-dependent changes in the localization of L-plastin (in actin aggregates) and cortactin (in the sealing ring) suggest that these proteins may be involved in the initial and maturation phases of sealing ring formation, respectively. siRNA to cortactin inhibits this maturation process but not the formation of actin aggregates. Osteoclasts treated as above but with TNF-α demonstrated very similar effects as observed with RANKL. Osteoclasts treated with a neutralizing antibody to TNF-α displayed podosome-like structures in the entire subsurface and at the periphery of osteoclast. It is possible that TNF-α and RANKL-mediated signaling may play a role in the early phase of sealing ring configuration (*i.e.* either in the disassembly of podosomes or formation of actin aggregates). Furthermore, osteoclasts treated with alendronate or αv reduced the formation of the sealing ring but not actin aggregates. The present study demonstrates a novel mechanistic link between L-plastin and cortactin in sealing ring formation. These results suggest that actin aggregates formed by L-plastin independent of integrin signaling function as a core in assembling signaling molecules (integrin αvβ3, Src, cortactin, etc.) involved in the maturation process.

Osteoclasts, the multinucleated and terminally differentiated giant cells, are involved in bone resorption. The adhesion of osteoclasts to the bone during bone resorption leads to the formation of the clear zone, an actin-rich ring-like adhesion zone circumscribing an area of bone resorption. Formation of a clear zone or sealing zone (also known as the sealing ring) has been considered to be a marker of osteoclast activation and is fundamental to the process of osteoclast bone resorption. Sealing ring formation is mediated by the dynamics of the actin cytoskeleton. Distinct pathways and signaling molecules have been shown to play roles in the organization of the sealing ring during bone resorption. Our previous observations in gelsolin null ($Gsn^{-/-}$)[2] osteoclasts demonstrated that deficiency of this protein blocks podosome assembly and motility. However, the cells still exhibit sealing ring and matrix resorption (1). Therefore, $Gsn^{-/-}$ osteoclasts are capable of resorbing bone, but the resorbed areas are small due to the absence of podosomes and the resulting hypomotile nature of osteoclasts (1). Observations in $Gsn^{-/-}$ osteoclasts also suggest that the organization of the sealing ring presumably reflect changes in the role of actin-binding proteins. Spatial configurations of actin filaments by actin-binding proteins (ABPs) account for the highly specific changes in cell shape during migration and bone resorption. ABPs assist in stabilizing and rearranging the organization of the actin cytoskeleton in response to external stimuli or during cell migration and adhesion. A few of the ABPs have been identified as having a role in osteoclast function (1–6).

Wiskott-Aldrich syndrome protein (WASP) is one of the ABPs, and it has a role in sealing ring formation and bone resorption in osteoclasts (7, 8). It is also a binding partner for c-Src family protein-tyrosine kinases (7, 9). Calle *et al.* (8) have demonstrated that osteoclasts from WASP knock-out mice failed to demonstrate a sealing ring, and these osteoclasts are less resorptive. Expression of WASP restores normal cytoarchitecture in these osteoclasts. Most recently, we have demonstrated that a phosphatase called PTP-PEST is involved in the dephosphorylation of Src at Tyr^{527} and phosphorylation of Src at Tyr^{418} in the catalytic site (10). This resulted in activation of Src and interaction of Src, cortactin, and Arp2/3 complex with WASP. WASP, which is identified in the sealing ring of resorbing osteoclasts, also exhibited interaction with Src, PYK2, cortactin, PTP-PEST, Pro-Ser-Thr phosphatase-interacting protein (PST-PIP), and Arp2/3 in immunostaining analyses (7). Furthermore, WASP integrates signals from Rho, Cdc42, and kinases to bind and stimulate actin polymerization and sealing ring formation in osteoclasts (5, 7, 10). Experiments with WASP peptides containing Pro-rich and $Tyr(P)^{294}$-containing peptides demonstrated significant effects on osteoclast signaling and sealing ring formation (11). Modulation of the phosphorylation state of WASP by kinase(s) assists in integrating multiple signaling molecules that play a part in the assembly of

* This work was supported, in whole or in part, by National Institutes of Health, NIAMS, Grant AR46292. This work was also supported by bridge funding provided by the American Society for Bone and Mineral Research.

[S] The on-line version of this article (available at http://www.jbc.org) contains supplemental Tables S1 and S2 and Figs. S1–S5.

[1] To whom correspondence should be addressed: University of Maryland, Dental School, Dept. of Oncology and Diagnostic Sciences, 650 W. Baltimore St., Baltimore, MD 21201. Tel.: 410-706-2083; Fax: 410-706-0865; E-mail: mchellaiah@umaryland.edu.

[2] The abbreviations used are: $Gsn^{-/-}$, gelsolin null; ABP, actin-binding protein; RANKL, receptor activator of NF-κB ligand; M-CSF, macrophage colony-stimulating factor; WASP, Wiskott-Aldrich syndrome protein; PTP-PEST, protein-tyrosine phosphatase-proline-glutamic acid-serine-threonine; ScRNAi, scrambled interference RNA.

the sealing ring. Integrin $\alpha v\beta 3$ signaling plays a key role in this process. We suggest this based on observations that osteoclasts treated with osteopontin, a ligand for $\alpha v\beta 3$, increase interaction of signaling proteins with WASP, formation of the sealing ring, and bone resorption (7).

Mounting evidence has demonstrated the ability of the integrin $\alpha v\beta 3$-mediated pathway to induce osteoclast activity and bone resorption. Formation of signal-generating complex consisting of Src, PYK2, focal adhesion kinase, $p130^{cas}$, c-Cbl, and PI3K associated with $\alpha v\beta 3$ has been shown to play roles in the organization of the sealing ring during bone resorption (7, 12–19) (for a review, see Ref. 20). An inhibitor to αv, RGD mimetics, and $\alpha v\beta 3$-blocking antibodies inhibit bone resorption *in vitro* and *in vivo*, suggesting that this integrin plays an important role in osteoclast function (21–23). Integrin $\alpha v\beta 3$-associated proteins integrate multiple signaling pathways and signaling molecules that partake in the assembly of the sealing ring during bone resorption and podosome assembly/disassembly during migration in osteoclasts.

The importance of TNF-α has been implicated in osteoclastogenesis and the bone loss that occurs in inflammatory diseases, such as rheumatoid arthritis and periodontitis (24–29). Fuller *et al.* (24) have shown that TNF-α potently directly activates osteoclasts, and actin rings were formed rapidly in response to minuscule concentrations of TNF-α. TNF-α was as potent as receptor activator of NF-κB ligand (RANKL) in osteoclast activation and even more effective in activation than osteoclast formation. It seems that TNF-α has the potentiality to act by itself and synergize with RANKL in osteoclast differentiation and bone resorption. Further investigations on the spatially and temporally regulated functions of actin-binding proteins and pathways are necessary to identify their role in actin cytoskeleton dynamics during bone resorption.

Osteoclasts may contain a variety of actin-binding proteins besides WASP, gelsolin, profilin, and Cap Z. However, it is not clear how these proteins specifically operate at the level of assembly of actin-related structures during bone resorption. The focus of this paper is to address how the sealing ring, a structure fundamental to the function of the osteoclast, is organized and regulated. Therefore, to identify the key proteins involved in sealing ring formation as well as to dissect the dynamic mechanisms that govern the formation of the sealing ring, we have used the novel proteomic approach to profile the key regulatory proteins in osteoclasts subjected to bone resorption. We have shown here that mouse osteoclasts incubated with native bone particles demonstrated a significant increase in cortactin and decrease in L-plastin as compared with osteoclasts not exposed to bone particles for 16–18 h in the presence of RANKL and M-CSF. Therefore, this increase is related to the bone resorption activity of osteoclasts. We have also shown here that formation of secondary actin adhesive aggregates represents part of the phenotypic changes observed prior to sealing ring formation on mineralized matrix. L-plastin has a regulatory role in the formation of this structure by its actin bundling property. An inhibitor to αv blocked sealing ring formation. However, these cells displayed actin aggregates. On the contrary, osteoclasts treated with a neutralizing antibody to TNF-α, and an inhibitor to Src demonstrated punctate podosome-like structures in the entire subsurface and at the periphery of the osteoclasts. Failure of formation of actin aggregates in these osteoclasts suggests that TNF-α-mediated signaling may have a role in the onset of sealing ring formation. Src may have roles at the early and late stage of sealing ring formation.

EXPERIMENTAL PROCEDURES

Reagents—Antibody to L-plastin (SC-16657), actin (SC-8432), GAPDH (SC-32233), $p130^{cas}$ (SC-859), PYK2 (SC-1514), WASP (SC-13139), c-Src (SC-8056), anti-phosphotyrosine (PY20; SC-508), αv (SC-6617), and $\beta 3$ (SC-6627) as well as siRNA to cortactin (SC-35093) and control RNAi (SC-44233) were bought from Santa Cruz Biotechnology, Inc. (Santa Cruz, CA). Phosphoserine antibody was purchased from Zymed Laboratories Inc., Inc. (San Francisco, CA). Cortactin (H222, catalog no. 3503) antibody was purchased from Cell Signaling Technology, Inc. (Danvers, MA). Antibodies to GAPDH and TNF-α (anti-mouse; catalog no. 10950) were bought from Abcam Inc. (Cambridge, MA). Recombinant TNF-α and M-CSF proteins and TNFR1 (TNF-α receptor 1) antibody were purchased from R & D Systems (Minneapolis, MN). Cyclo-RGD peptide (catalog no. PCI-3661-P1) was purchased from Peptides International (Louisville, KY). Protein estimation reagent, molecular weight standards for proteins, and PAGE reagents were bought from Bio-Rad. Cy2- and Cy3-conjugated secondary antibodies were purchased from Jackson Immunoresearch (West Grove, PA). HRP-conjugated secondary antibodies for immunoblotting were obtained from GE Healthcare. pEGFP-actin vector was bought from Clontech. Rhodamine-phalloidin and other chemicals were purchased from Sigma.

Preparation of Osteoclast Precursors from Mice—C57/BL6 mice were used for osteoclast preparation as described previously (7). These mice were either purchased from Harlan Laboratory or generated in the animal facility of the University of Maryland Dental School. Breeding and maintenance were carried out as per the guidelines and approval of the institutional animal care and use committee. Osteoclasts were generated *in vitro* using mouse bone marrow cells as described previously (7).

Purification of Glutathione S-Transferase (GST)-fused RANKL—pGEX vector containing RANKL cDNA was expressed in *Escherichia coli* as GST fusions as described previously (30). SDS-PAGE and Coomassie Blue staining tested the purity of the RANKL. Accurate protein content of the purified RANKL protein was determined by densitometric quantification of the protein bands separated by SDS-PAGE using known concentrations of BSA as a standard.

Preparation of Osteoclast Lysate after Various Treatments—After flushing the marrow cells for osteoclast differentiation, mouse long bones (free of cells inside and muscles outside) were washed extensively with PBS and kept in ethanol until use. Long bones were air-dried in hood and homogenized by a miniblender. Bone particles were sieved, and bone particles 60–80 μm in size were used for experiments. The multinucleated osteoclasts were seen from day 4 onward, as shown in Fig. 2. At this stage, osteoclasts were added with sterile native bone particles. 100 μg of bone particles were added to a well of 6-well cell culture plates. Three to four wells were used per condition.

Osteoclasts were treated with (+) and without (−) bone particles for 16–18 h in the presence of macrophage colony-stimulating factor (10 ng/ml) and RANKL (50–60 ng/ml).

Some cultures were treated with mouse TNF-α (20 ng/ml) and bisphosphonates (alendronate or pamidronate, 50 μM) at 37 °C. Bisphosphonate stocks (1 mM) were made in PBS or sterile H_2O (31). Cells were treated with bisphosphonates in the presence of bone particles, M-CSF, and RANKL. Prior to the addition of TNF-α, osteoclasts generated with RANKL and M-CSF were washed extensively with serum-free alpha-minimum essential medium and incubated with the same for 30 min. Subsequently, adherent cells were detached with stripping solution (catalog no. 25056-CL; Cellgro by Media Tech, Inc., Herndon, VA) as described previously (32). Cells were replated in MEM containing 10% fetal bovine serum (FBS), M-CSF and TNF-α. Cultures treated with TNF-α do not contain RANKL. Based on dose-dependent studies, cells were neutralized with 40–50 ng/ml TNF-α antibody (goat polyclonal anti-mouse TNF-α; catalog no. ab10950, Abcam) and 3–5 μg/ml anti-mouse TNFR1 (MAB430) antibody. To enhance the blocking effect, cells were preincubated with the antibody of interest for 60–90 min prior to the addition of TNF-α and M-CSF. Incubation was continued for 12–14 h for the bone resorption assay and immunostaining analyses. Normal serum was used as a control for the antibody treatment. We have performed a trypan blue dye (Sigma T8154) exclusion test to determine the viability of osteoclasts after various treatments. Cells demonstrated clear cytoplasm with no inclusion of blue dye. Osteoclasts were viable after various treatments, such as bone particles, bisphosphonates, αv inhibitor, Src inhibitor, and anti-TNF-α.

Following various treatments, osteoclasts were washed three times with cold PBS and lysed in a radioimmune precipitation buffer (10 mM Tris-HCl, pH 7.2, 150 mM NaCl, 1% deoxycholate, 1% Triton X-100, 0.1% SDS, 1% aprotinin, 2 mM PMSF, 100 μM Na_3VO_4, and 1% aprotinin), as described previously (33). Cells were rocked on ice for 15 min and scraped off with a cell scraper. Cell lysates were centrifuged at 15,000 rpm for 5 min at 4 °C, and the supernatant was saved. Protein contents were measured using Bio-Rad protein assay reagent.

SDS-PAGE and Western Analysis—About 50–100 μg of protein was used for 10% SDS-PAGE. After electrophoresis, the gels were washed and stained with Coomassie Brilliant Blue for 2–3 h as described previously (34). About 100–150 μg of protein was used for immunoblotting analysis. The proteins were transferred to a PVDF membrane for Western analysis. Blots were blocked with 10% milk in PBS containing 0.5% Tween (PBS-T) for 2–3 h and then incubated with 1:1000 dilutions of primary antibody of interest for 2–3 h. After three washes for 10 min each with PBS-T, the blot was incubated with a 1:1000 dilution of peroxidase-conjugated species-specific respective secondary antibody for 2 h at room temperature. After three washes for 10 min each with PBS-T, protein bands were visualized by chemiluminescence using the ECL kit (Pierce). Blocking and immunoblotting were performed with 5% BSA in PBS-T for phosphotyrosine antibody (PY20) (32).

Immunohistochemistry and Actin Staining—Osteoclast precursors (10^5 cells/coverslips) were cultured on dentine slices and incubated for different time periods as indicated in Figs. 1, 5, 6, and 7. Osteoclasts were fixed with 3% paraformaldehyde for 20 min and permeabilized with 0.1% Triton X-100 in PBS for 5 min as described previously (5). Background fluorescence was blocked by incubating cells with either 5% horse serum or 5% BSA in PBS for 30–45 min at 4 °C. The cells were washed and incubated with primary antibodies (cortactin, β3, or L-plastin) of interest (1:100 dilutions) in the blocking solution for 2 h at 4 °C. The primary antibodies were detected with either Cy2- or FITC-conjugated secondary antibody (1:100 dilutions). Cells stained for cortactin, β3, or L-plastin were stained for actin with rhodamine-phalloidin, as described previously (35). The cells were washed and mounted on a slide in a mounting solution (Vector Laboratories) and sealed with nail polish. Immunostained osteoclasts were photographed with a Bio-Rad confocal laser-scanning microscope. Images were stored in TIF image format and processed by Adobe Photoshop (Adobe Systems Inc., Mountain View, CA).

Actin Staining with Rhodamine-Phalloidin—Cells were fixed and permeabilized with 3.7% paraformaldehyde and 0.1% Triton X-100 for 10 min. Cells were then washed with PBS containing 5 mM EGTA (PBS/EGTA) and stained for actin with rhodamine-phalloidin (1:1000 dilution; Sigma) as described previously (2). Actin-stained cells were viewed and photographed on a Bio-Rad confocal laser-scanning microscope. Images were stored in TIF image format and processed by Adobe Photoshop (Adobe Systems Inc.). Sealing (actin) rings were counted in osteoclasts (~300–350), and significance was calculated as described below.

Bone Resorption Assay in Vitro—Bone resorption assay was performed as described previously (37). Osteoclasts were cultured on dentine slices and incubated for 16–18 h. Subsequently, dentine slices were scanned in confocal microscopy to determine the resorbed area. Images were stored in TIF format and processed by Adobe Photoshop (Adobe Systems Inc.).

Statistical Analysis—All values were mean ± S.E. of three or more experiments done at different times normalized to intraexperimental control values. A value of <0.05 was considered significant. For statistical comparisons, analysis of variance was used with Bonferroni corrections (INSTAT for IBM version 2.0, GraphPad software).

RESULTS

Analysis of Time-dependent Changes in Cytoskeletal Organization during Bone Resorption

During the process of bone resorption, osteoclasts undergo reorganization of actin cytoskeleton. Some of the earlier mechanisms required for generation and maturation of the sealing zone have not been studied. Therefore, we proceeded to establish the sequential changes in the morphology and organization of actin filaments in osteoclasts subjected to bone resorption *in vitro*. Osteoclasts plated on dentine slices were fixed at the indicated time and stained with rhodamine-phalloidin for actin. Fig. 1 illustrates time-dependent changes in the organization of actin cytoskeleton. Between 1 and 3 h, osteoclasts begin to spread on bone by adhering to the bone surface through the formation of secondary actin aggregates, which function as secondary adhesive

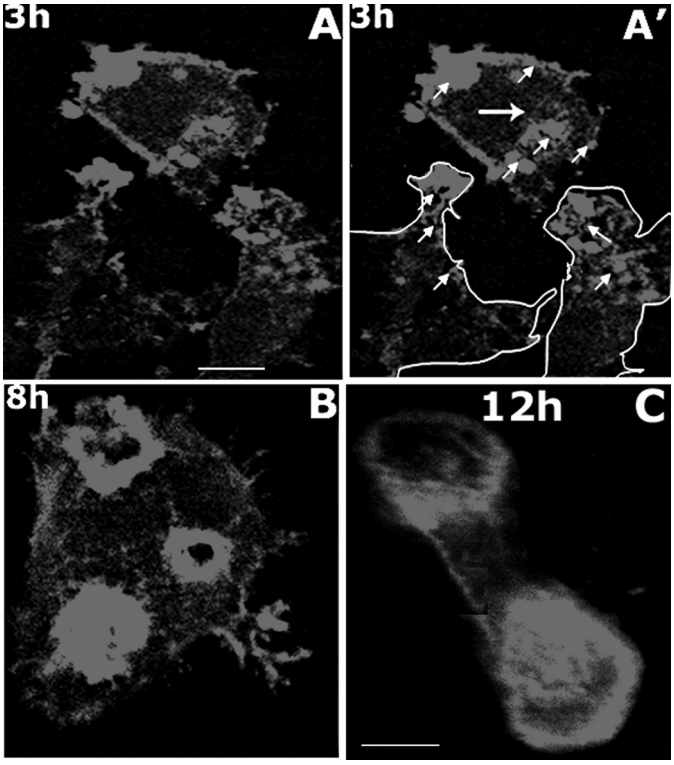

FIGURE 1. **Analysis of actin distribution in osteoclasts subjected to bone resorption.** Osteoclasts plated on dentine slices for 3 h (*A* and *A′*), 8 h (*B*), and 12 h (*C*) were stained with rhodamine-phalloidin to determine the changes in the distribution of actin during bone resorption. Osteoclasts are outlined in *A′* to indicate stretching off of membrane at 2–3 h. Actin aggregates that most likely function as secondary adhesive structures are indicated by *arrows* in *A′*. An increase in the number of actin rings (*B* and *C*) was observed as a result of the increased surface area of osteoclasts at 8 and 12 h. *Scale bars*, 25 μm. The results are representative of four experiments with four separate osteoclast preparations.

structures (indicated by the *arrows* in Fig. 1*A′*). These structures provide traction for membrane extensions, as shown in Fig. 1*A*. Cells are outlined in Fig. 1*A′*. Formation of secondary actin aggregates and spreading of osteoclasts increase the surface area of osteoclasts (Fig. 1, *A*–*C*). These secondary adhesive structures are different from typical podosome structures observed in osteoclasts during adhesion and migration (1, 36). Maturation of actin aggregates to the sealing ring takes place from 6 h onwards. Osteoclasts exhibit either single or multiple mature and functional sealing rings between 8 and 12 h (Fig. 1, *B* and *C*).

Osteoclasts Migrated toward and Adhered to the Native Long Bone Particles

Osteoclasts subjected to bone resorption undergo considerable changes in morphology due to reorganization of actin cytoskeleton, as shown in Fig. 1. Therefore, we determined the changes in morphology of osteoclasts incubated with native bone particles (Fig. 2). Osteoclast precursors were observed on day 4 or 5 in culture (Fig. 2*B*). Native long bone particles of mice (60–80 μm; Fig. 2*A*) were added to cells at this stage (100 μg/well in a 6-well cell culture plate) for 16–18 h in the presence of RANKL (40–50 ng/ml) and M-CSF (10 ng/ml), as described under "Experimental Procedures." Pictures were taken in an inverted phase-contrast microscope (Fig. 2, *A*–*D*). Migration of osteoclasts toward the particles was observed at

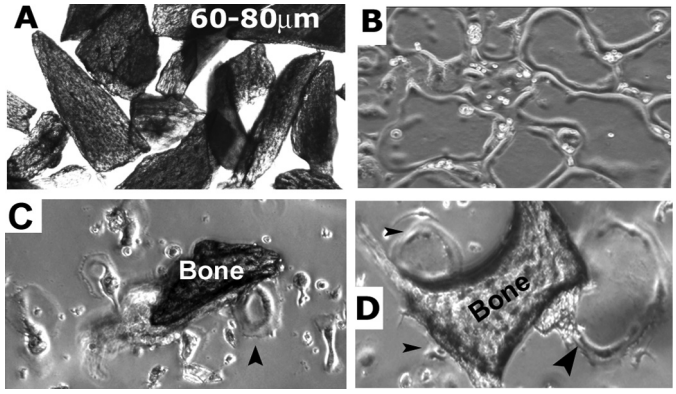

FIGURE 2. **Analysis of cell shape changes in osteoclasts incubated with native long bone particles.** *A*, bone particles (~60–80 μm in size) isolated from the long bones of mice. *B*, confluent osteoclast in culture prior to bone treatment is shown. Osteoclasts were incubated with bone particles (60–80 μm size) for 4 h (*C*) and 6 h (*D*). The *arrowheads* in *C* and *D* indicate osteoclasts that are attached to bone particles. These osteoclasts are capable of forming actin ring and bone resorption. Osteoclasts were viewed under a ×40 objective in an inverted microscope. Experiments were repeated with more than 10 different osteoclast preparations. The data shown are representative of those experiments.

2 h (*C*), and attachment of osteoclasts to bone was observed at 4 h (*D*). Osteoclasts attached to bone particles were indicated by *arrowheads* (*C* and *D*). Similar observations were found in short term live cell analysis of osteoclasts expressing GFP-actin and incubated with dentine slices (supplemental Fig. S1, *A* and *B*).

Analysis of Expression Profile of Proteins in Osteoclasts Subjected to Bone Resorption

Lysates (~50 μg) made from osteoclasts incubated with (+) and without (−) bone particles for 16–18 h in the presence of RANKL and M-CSF were used for SDS-PAGE and Coomassie Blue staining (Fig. 3*A*). A dramatic increase in 80–85-kDa protein and a decrease in 65-kDa protein were observed (Fig. 3*A*, *lanes 1* and *2*). These proteins were identified as cortactin and L-plastin by immunoblotting analyses with respective antibodies (Fig. 3*A*, *lanes 3* and *4*). Lysates (500 μg) made from osteoclasts treated with or without bone particles were subjected to two-dimensional gel electrophoresis (supplemental Figs. S2 and S3). Two-dimensional gel electrophoresis and mass spectrometry (MS) analyses corroborate the above findings. The major spots in two-dimensional gel electrophoresis were digested, and the peptides were subjected to MS analysis. A trace yielded about 15–17 matching peptide masses, representing about 30–35% coverage for L-plastin (supplemental Table S1, under (−) Bone). Peptide sequences identified in MS are *highlighted* in *red* in supplemental Fig. S3*A*. A representative mass spectrum (FSLVGIAGQDLNEGNR) is provided in supplemental Fig. S3*B*. Similarly, a trace yielded about 25–31 matching peptide masses, representing about 19–22% coverage for cortactin (supplemental Table S1) in osteoclasts treated with bone particles (supplemental Table S1, under (+) Bone).

Because there is a decrease in the level of L-plastin at 16–18 h, we extended this analysis to determine the L-plastin levels at different time periods after the addition of bone particles in the presence of RANKL and M-CSF. Immunoblotting with an antibody to L-plastin was performed with ~50 μg of lysate protein.

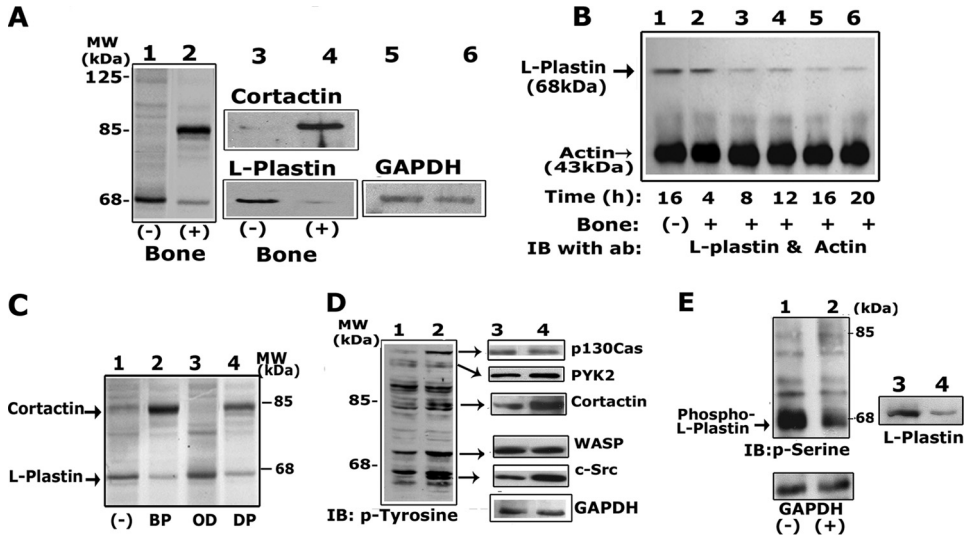

FIGURE 3. **Analysis of the expression profile of proteins in osteoclasts treated with and without native bone particles.** *A*, treatments of osteoclasts with bone particles were performed as described under "Experimental Procedures." *Lanes 1* and *2*, lysate proteins made from osteoclasts incubated with (+) and without (−) bone particles for 16–18 h were subjected to 10% SDS-PAGE and Coomassie Blue staining analyses. *Lanes 3* and *4*, immunoblotting analysis with a cortactin (*top*) and L-plastin antibody (*bottom*). *B*, osteoclasts were treated with bone particles for different time periods as indicated at the *bottom*. Lysates were separated on SDS-polyacrylamide gels and then transferred and probed with L-plastin and actin antibodies sequentially without stripping. *C*, equal amounts of lysate proteins from osteoclasts treated as indicated in the figure were subjected to SDS-PAGE and Coomassie Blue staining. (−), untreated osteoclasts; *BP*, bone particles; *OD*, osteologic discs; *DP*, dentine particles. *D*, equal amounts of protein lysates made from osteoclasts treated with (*lanes 2* and *4*) and without (*lanes 1* and *3*) bone particles were subjected to three SDS-10% polyacrylamide gels. Blots made from these three gels were immunoblotted with anti-Tyr(P) (*p-Tyrosine*), p130^{cas}, and PYK2 antibody, respectively. These blots were stripped and blotted correspondingly with GAPDH/cortactin, WASP, and Src antibody. Immunoblotting of the first blot with GAPDH (37 kDa) and cortactin (80–85 kDa) antibody was performed sequentially without any further stripping. *E*, immunoblotting (*IB*) analysis with a Ser(P) (*p-serine*) antibody. This immunoblot was sequentially probed with a Ser(P), L-plastin, and GAPDH antibody. Immunoblotting analysis with a GAPDH (*A*, *D*, or *E*) or actin (*B*) antibody was used as a loading control. The results are representative of three experiments performed with three separate osteoclast preparations.

Immunoblotting of the same blot with an actin antibody after stripping was used as a loading control. A decrease in the level of L-plastin was observed from 8 h onward (Fig. 3*B*, *lanes 3–6*) and remained unchanged until 20 h (*lane 6*). The decrease at 16–20 h corresponds with the decrease shown in Fig. 3*A*. These results suggest that changes in the levels of L-plastin occur at the early stage of bone resorption could be correlated with the dynamic nature of the sealing ring.

Analysis of Protein Profile in Osteoclasts Incubated with Different Substrates

Osteoclasts can attach to various substrates, such as glass, synthetic mineralized materials (*e.g.* osteologic discs), and mineralized bone (*e.g.* dentine, ivory, and natural bone). We have used previously (1, 10, 11) and at this time biologically derived hard tissues, such as devitalized native bone or dentine slices, as substrates for *in vitro* bone resorption assays. Researchers also use osteologic discs containing submicron calcium phosphate films (~0.6 μm) on transparent quartz material (BD Biosciences) for *in vitro* bone resorption assays. Therefore, we explored whether the aforesaid substrates are biologically comparable and exhibit a very similar effect, as shown in Figs. 1–3. We have observed migration of osteoclasts toward native devitalized bone particles (Fig. 2*C*) and dentine (supplemental Fig. S1) but not toward osteologic discs. Therefore, osteoclasts were cultured on the surface of osteologic discs and incubated in the presence of RANKL (40–50 ng/ml) and M-CSF (10 ng/ml) for 16–18 h. SDS-PAGE was performed with lysates made from osteoclasts treated with the indicated substrates (Fig. 3*C*) for 16–18 h. Osteoclasts under the same conditions as above but untreated with any of the indicated substrates were used as controls (Fig. 3*C*, *lane 1*). Although the geometry of bone and dentine surfaces could be different, a very similar protein profile was observed in SDS-PAGE analysis (*lanes 2* and *4*). However, the protein profile of lysates made from osteoclasts incubated on osteologic discs (*lane 3*) does not correspond with these profiles (*lanes 2* and *4*). Osteologic discs lack bone matrix proteins and the geometry of dentine or bone particles. It is possible that synthetic mineralized matrices were quickly resorbed by mature osteoclasts within 4–6 h of incubation. We have observed osteoclasts attached on the quartz disc at this time period after the completion of resorption of the calcium phosphate matrix (data not shown). This could be the possible reason for a relatively similar protein profile in osteoclasts untreated with bone particles (*lane 1*) or plated on osteologic discs (*lane 3*).

Analysis of the Phosphoprotein Profile in Osteoclasts Incubated with Bone Particles

Two-dimensional gel electrophoresis and MS analyses of lysates made from osteoclasts incubated with bone particles demonstrated peptides for a few of the proteins (Src kinase, vacuolar H^+-ATPase B2, vacuolar ATP synthase catalytic subunit A, L-plastin, cathepsin D and K, Arp2/3, cortactin, and gelsolin) identified as being involved in bone resorption. In order to gain insight into the signaling molecules involved in osteoclast bone resorption in general, we looked at the phosphorylation state of proteins on tyrosine and serine residues. We used ~250 μg of lysate protein for immunoblotting analyses (Fig. 3, *D* and *E*). Immunoblotting analysis with an antibody to phosphotyrosine (Fig. 3*C*) displayed an increase in the phosphorylation of p130^{cas}, cortactin, WASP, and c-Src in osteoclasts treated with bone particles. Minimal changes in the tyrosine phosphorylation of PYK2 were observed (Fig. 3*D*, *lanes 1* and *2*). This status might not exclude the role PYK2 in osteoclast function. Phosphorylation may perhaps occur at the early stage of maturation of the sealing ring from actin aggregates. PYK2-dependent podosome belt formation in PYK2 null osteoclasts has been shown to occur by the kinase-defective mutant. It is also possible that PYK2 may function as a platform for

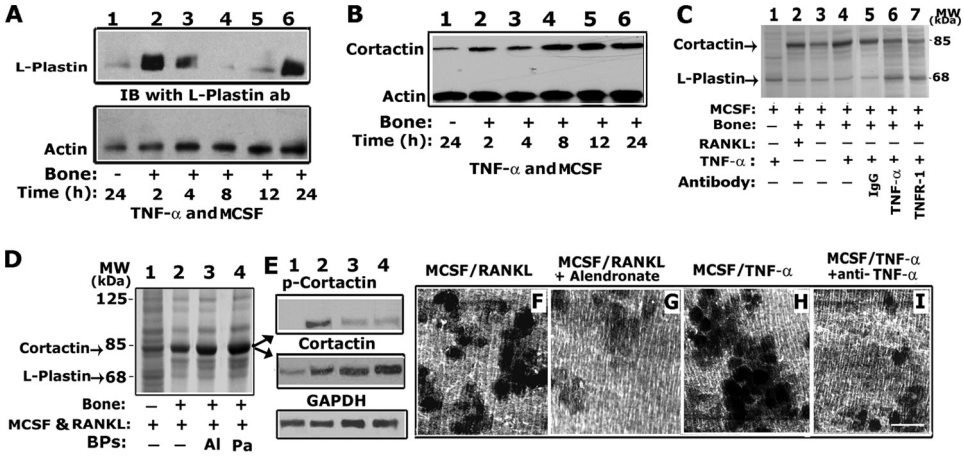

FIGURE 4. **SDS-PAGE and immunoblotting analyses of lysates made from osteoclasts subjected to various treatments.** *A* and *B*, time-dependent effects of TNF-α on L-plastin and cortactin levels. Equal amounts of lysate proteins were used for immunoblotting analysis with an antibody (*ab*) to L-plastin (*A*) and cortactin (*B*). Actin was used as a loading control in *A* and *B*. *C*, equal amounts of lysate proteins from osteoclasts treated as indicated in the figure were subjected to SDS-PAGE (10%) and Coomassie Blue staining analyses. *MCSF*, macrophage colony-stimulating factor; (−) and (+), untreated and bone particle-treated; *IgG*, control nonspecific IgG control; *TNFR1*, anti-TNF-1 receptor. *D* and *E*, equal amount of lysate proteins from osteoclasts treated with various treatments, as indicated in the figure, were used for SDS-PAGE/Coomassie Blue staining (*D*) and immunoblotting analyses (*E*). Immunoblotting analyses with phosphocortactin (Tyr(P)^{421}) (*E*, *top*, *p-Cortactin*), cortactin (*E*, *middle*), and GAPDH (*E*, *bottom*) are shown. *F–I*, bone resorption assay *in vitro*. Osteoclasts were treated as indicated at the *top* of each *panel* (*E–F*). Pits were scanned under confocal microscopy. Resorption pits were seen as dark spots. *Scale bar*, 25 μM. These results represent one of three separate experiments performed with the same results.

recruitment and assembly of signaling proteins besides its function as a kinase (37). An increase in the tyrosine phosphorylation of c-Src and cortactin (Fig. 3*D*, *lanes 1* and *2*) corresponds with the protein levels in osteoclasts treated with bone particles (*lanes 3* and *4*). However, equal levels of WASP, PYK2, and p130^{cas} proteins were observed in osteoclasts untreated and treated with bone particles (Fig. 3*D*, *lanes 3* and *4*). This observation confirms the previous observations of ours and others that an increase in the phosphorylation of several signaling proteins is necessary for osteoclast bone resorption (6, 7, 14, 18, 38).

Immunoblotting analysis with a phosphoserine antibody showed a decrease in the phosphorylation state of L-plastin in osteoclasts treated with bone particles (Fig. 3*E*, *lane 2*). This corresponds with the decreased protein level of L-plastin (Fig. 3*E*, *lane 4*). Immunoblotting analysis with a GAPDH antibody demonstrated the same levels of GAPDH protein (Fig. 3, *A*, *D*, and *E*). Overall, these results demonstrate a decrease in L-plastin and an increase in cortactin in osteoclasts incubated with native bone particles for 16–18 h in the presence of RANKL and M-CSF.

Analysis of the Effects of TNF-α on the Protein Profile in Osteoclasts Subjected to Bone Resorption

TNF-α is sufficient to induce osteoclast differentiation and bone resorption independently of the RANKL signaling pathway (19, 20, 39–42). Chronic inflammatory bone diseases, such as rheumatoid arthritis, periodontal disease, and aseptic periprosthetic osteolysis are characterized by bone loss around affected joints and teeth caused by increased osteoclastic bone resorption. This resorption is mediated largely by the increased local production of TNF-α (42). Therefore, we checked whether TNF-α could induce effects similar to that of RANKL in osteoclasts subjected to bone resorption with bone particles for the times indicated in Fig. 4 (*A* and *B*). An equal amount (~50 μg) of lysate protein made from osteoclasts incubated with (+) and without (−) bone particles in the presence of TNF-α and M-CSF was used. Immunoblotting analysis was performed with L-plastin (Fig. 4*A*) and cortactin (Fig. 4*B*) antibody. We have observed a time-dependent increase in L-plastin level at 2 and 4 h. A decrease was observed from 8 h onward, and the decrease was stabilized until 12–20 h and then increased at 24 h. Time-dependent changes in the levels of L-plastin protein correspond with the phosphorylation level of L-plastin on serine residues (data not shown). However, cortactin level remains the same in osteoclasts untreated for 24 h (*B*, *lane 1*) and treated (*lanes 2* and *3*) with bone particles for 2 and 4 h. A gradual increase in the level of cortactin was observed from 8 h onward, and this increase was stabilized until 24 h.

As shown in Fig. 4, TNF-α (Fig. 4*C*, *lane 4*) reproduced the effects mediated by RANKL (*lane 2*) in the presence of bone particles for 16–18 h. An increase in the levels of cortactin with a corresponding decrease in L-plastin was observed under these conditions (*lanes 2* and *4*) as compared with osteoclasts treated with M-CSF only in the presence of bone particles (*lane 3*) or both M-CSF and TNF-α in the absence of bone particles for 16–18 h (*lane 1*). Osteoclasts were pretreated with an antibody to TNF-α (*lane 6*) or TNF receptor (*lane 7*) for 60–90 min prior to the addition of bone particles, TNF-α, and M-CSF as described under "Experimental Procedures." Osteoclasts treated as above with antibody failed to show a decrease in L-plastin level. The level remains the same as in control osteoclasts untreated with bone particles but treated with TNF-α and M-CSF (Fig. 4*C*, *lane 1*). However, a small increase in the level of cortactin was observed in these cells (*lanes 6* and *7*). Treatment of osteoclast with species-specific IgG (*lane 5*) serves as a control for TNF-α antibody treatment (*lane 6*). The response to TNF-α antibody was not observed in osteoclasts treated with IgG. Thus, the failure of anti-TNF-α/TNFR1 treatment to alter L-plastin levels suggests that TNF-α/TNFR1 signals mediate the early phase of sealing ring formation.

Analysis of the Effects of Bisphosphonates on the Protein Profile in Osteoclasts Subjected to Bone Resorption

Bisphosphonates inhibit bone resorption by osteoclasts (43–46). We recently reported that bisphosphonates could modulate the function of osteoclasts by inhibiting the tyrosine phos-

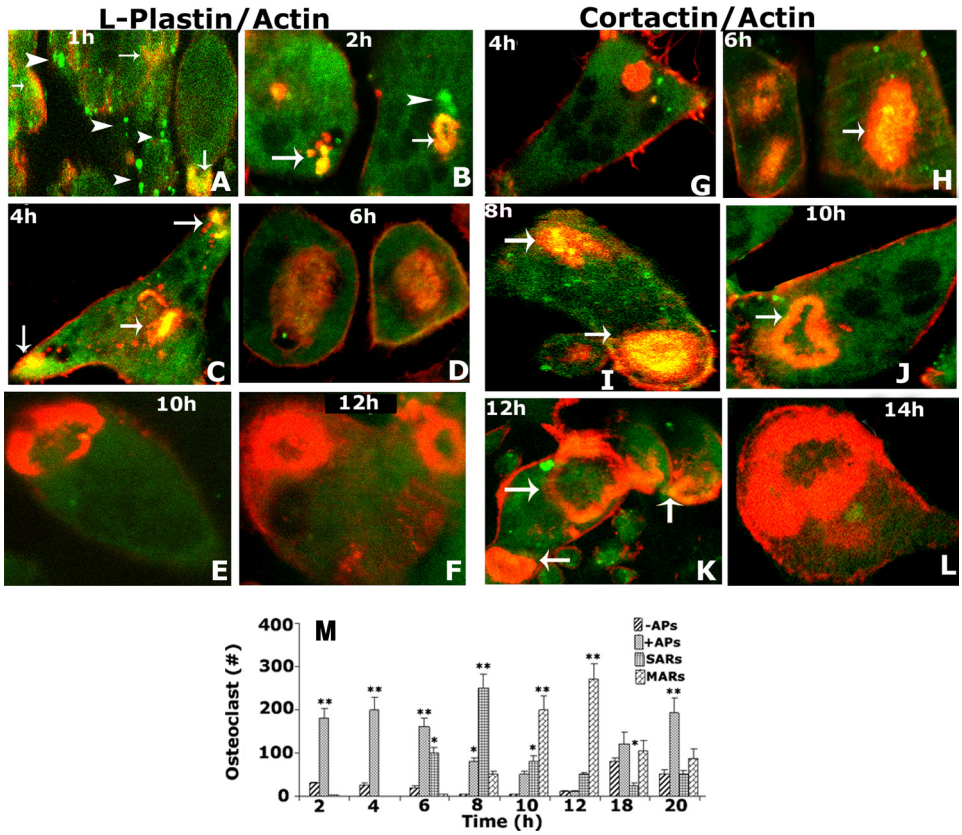

FIGURE 5. **Confocal analysis of time-dependent changes in actin organization and localization of L-plastin and cortactin in resorbing osteoclasts.** *A–L*, confocal microscopic images of osteoclasts stained for actin (*red*), L-plastin (*green*; *A–F*), and cortactin (*green*; *G–L*) are shown. *Yellow color* (indicated by *arrows*) represents the colocalization of proteins (*A–C* and *H–J*). *M*, changes in actin organization were determined in ~300 osteoclasts and provided as a *graph*. Measurements were performed at the indicated time *below* the *graph*. Shown is basic actin staining with no actin patches or aggregates (−*APs*), with actin patches or aggregates (+*APs*), with small actin rings (*SARs*), and with multiple or single big mature actin rings (*MARs*). Data are provided as mean ± S.E. of three experiments. **, $p < 0.001$; *, $p < 0.05$ *versus* cells with no actin patches.

phorylation of cortactin by regulating the activity of PTP-PEST and Src kinase (10). Consistent with this observation, immunoblotting analysis with a phosphospecific antibody to cortactin Tyr^{421} demonstrated a significant decrease in the $Tyr(P)^{421}$ phosphorylation (Fig. 4*E*, *top*, *lanes 3* and *4*) and not the level of cortactin in osteoclasts treated with alendronate (*Al*) and pamidronate (*Pa*) in the presence of bone particles, RANKL, and M-CSF (Fig. 4*E*, *middle*, *lanes 3* and *4*). SDS-polyacrylamide gel stained with Coomassie Blue corroborates this observation (Fig. 4*D*, *lanes 3* and *4*).

Bone Resorption Assay in Vitro

Furthermore, we confirmed the stimulatory and inhibitory effects of TNF-α and alendronate on osteoclast bone resorption *in vitro* (Fig. 4, *F–I*). The effects of RANKL (Fig. 4*F*) and TNF-α (Fig. 4*H*) on the stimulation of bone resorption activity of osteoclasts *in vitro* are blocked by alendronate (Fig. 4*G*) and anti-TNF-α (Fig. 4*I*), respectively. Taken together, these observations corroborate the role of TNF-α in osteoclast function as shown by others (39, 42). A decrease in the phosphorylation of cortactin at Tyr^{421} (Fig. 4*E*) and the presence of actin aggregates in osteoclasts treated with alendronate (31) suggest that bisphosphonates could modulate the function of osteoclasts by inhibiting integrin αvβ3 downstream signaling involved in tyrosine phosphorylation of cortactin (10). This could be separate from the Rho GTPase pathway (44).

Analysis of Time-dependent Changes in Actin Organization in Osteoclasts Subjected to Bone Resorption

The experiments shown in Figs. 3 and 4 indicate a clear association of L-plastin and cortactin to osteoclast bone resorption. We sought to determine the spatiotemporal organization of L-plastin and cortactin in osteoclasts plated on dentine slices by immunostaining and confocal analyses (Fig. 5). It is of particular interest to determine whether the changes in the levels and localization of L-plastin and cortactin are in fact associated with the reorganization of actin structures in resorbing osteoclasts. Immunostaining of osteoclasts plated on dentine slices were performed with L-plastin (Fig. 5, *A–F*) and cortactin (Fig. 5, *G–L*). Costaining with rhodamine-phalloidin was performed to determine the actin localization. Higher magnification images of osteoclasts exhibiting changes in actin organization are shown. Changes in the actin distribution were determined at different time points in ~300 osteoclasts and provided as a *graph* in Fig. 5*M*. We have observed a spatiotemporal change in the sealing ring organization and composition (*i.e.* localization of L-plastin and cortactin) in a time-dependent manner as described below.

L-Plastin/Actin Distribution—Besides diffuse distribution, L-plastin localization was also observed as patches or aggregates (indicated by *arrowheads*) within 1 h (Fig. 5*A*) of plating mature osteoclasts on dentine. Colocalization of L-plastin and actin was observed in some of these aggregates (indicated by the *arrows* in Fig. 5, *A* and *B*). These aggregates develop into larger sizes in a time-dependent manner from 2 to 4 h (Fig. 5, *B* and *C*). Multiple big and small actin aggregates were observed at 4 h. Colocalization (*yellow*) of L-plastin and actin was observed in these aggregates (Fig. 5*C*). Actin aggregates fuse together by 6 h (Fig. 5*D*), at which time localization of L-plastin in these structures is reduced, but diffuse distribution of L-plastin was observed throughout the osteoclast (Fig. 5*D*). A gradual decrease in the localization of L-plastin (Fig. 5, *E* and *F*) accompanies cortactin localization in actin aggregates and maturation of sealing ring formation. Actin aggregate formation corroborates the actin staining shown in Fig. 1. These data indicate that the actin aggregates or patches are possible precursors or presealing zone for the mature sealing ring.

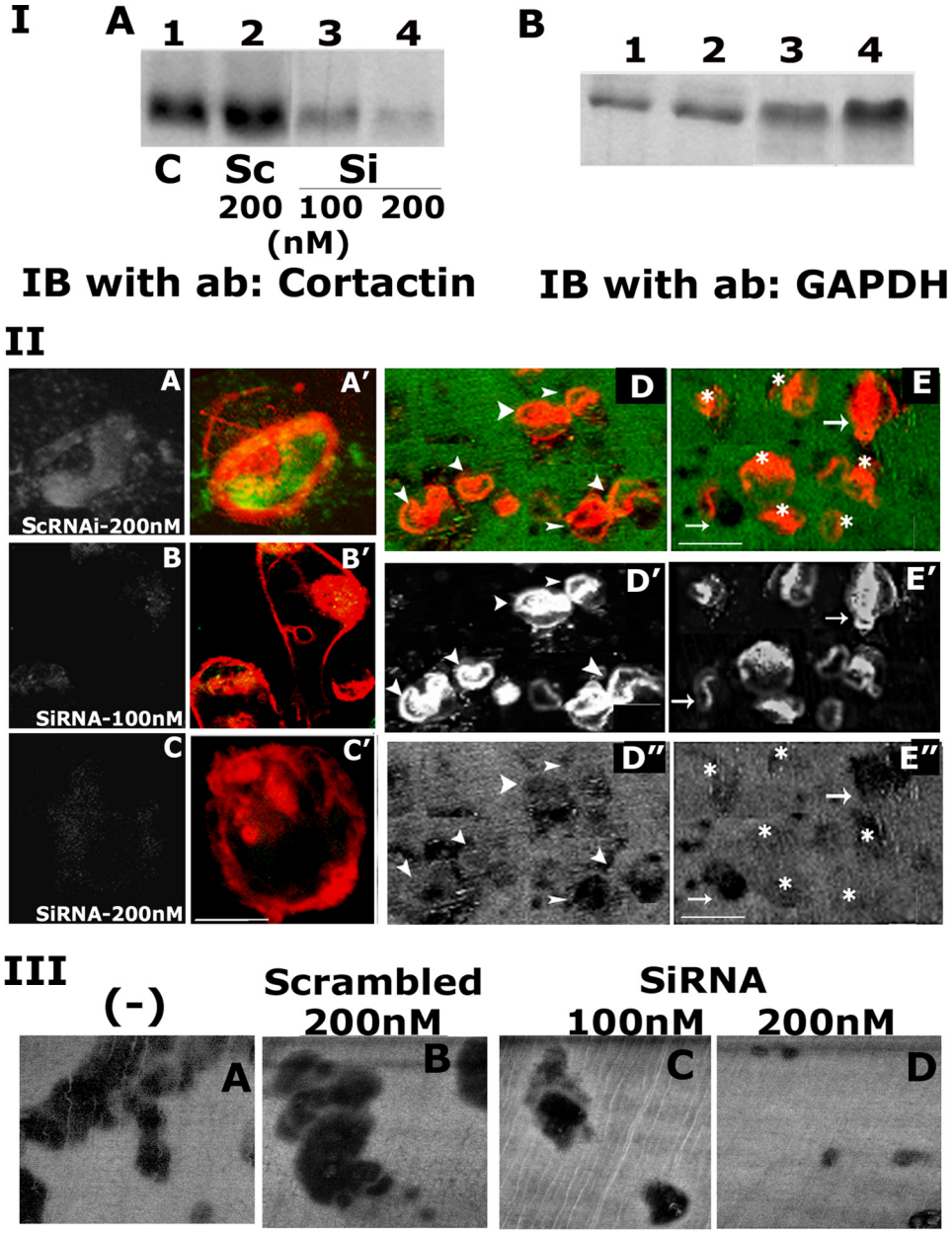

FIGURE 6. **Analysis of the effects of depletion or knockdown of cortactin on sealing ring formation and bone resorption.** *I*, immunoblotting analysis of cortactin levels in osteoclasts treated with control RNAi (*Sc*; 200 nM) and siRNA (*Si*; 100 and 200 nM) to cortactin (*A*). Immunoblotting analysis with GAPDH is shown in *B*. *II*, the effects of ScRNAi (*A* and *D*) and siRNA (*B*, *C*, and *E*) to cortactin on sealing ring formation. Osteoclasts were stained for cortactin (*green*) and actin (*red*). Cortactin distribution is shown in *A*–*C*. The effects of scrambled RNAi and SiRNA on multiple osteoclasts are shown in *D* and *E*. Osteoclasts were stained for actin (*red*) with rhodamine-phalloidin. Dentine is shown by the reflected light (*green* in *D* and *E*). Resorption pits were found underneath osteoclasts (*D*, *D*″, *E*, and *E*″). Actin distribution (*D*′ and *E*′) and resorption lacuna (*D*″ and *E*″) are shown separately in *gray*. Actin aggregates and superficial pits are indicated by *asterisks* in *E* and *E*″. Sealing rings are indicated by *arrowheads* (*D* and *D*′) and *arrows* (*E* and *E*′). *Scale bar*, 25 μm. *III*, bone resorption assay *in vitro*. Osteoclasts treated with scrambled ScRNAi and siRNA were cultured on dentine for 24 h. Pits were scanned in a confocal microscopy. Resorption pits were seen as *dark spots*. Experiments were repeated three times with three different osteoclast preparations. These results represent one of three separate experiments performed with the same results.

Cortactin/Actin Distribution in Sealing Ring—Distribution of cortactin in actin aggregates is very minimal or not observed at 4 h (Fig. 5*G*). Localization of cortactin was observed from 5 to 6 h onward (Fig. 5*H*) with a concomitant decrease in the localization of L-plastin (Fig. 5*D*). An increase in the localization of cortactin corresponds with the maturation of actin aggregates to the sealing ring between 8 and 10 h (*I* and *J*). A gradual decrease in the localization of cortactin was observed from 12 h onward (*K*), and at 14 h, cortactin was not observed in the mature actin ring, although diffuse distribution of cortactin was observed in these cells (*L*). The time-dependent changes in actin organization in osteoclasts expressing GFP-actin (supplemental Fig. S1) correspond with the changes shown in fixed cells (Fig. 5). Individual frames of the osteoclasts at 2–4, 4–6, and 10–12 h time periods are shown. Actin aggregates were formed at 4–6 h, and maturation of actin aggregates into a functional sealing ring was observed at 10–12 h (supplemental Fig. S1, *SR* in *C*′). Cells spread well on the bone at this time (supplemental Fig. S1*C*), and a resorption pit (supplemental Fig. S1, *2* in *C*″) was found underneath the sealing ring (supplemental Fig. S1*C*).

Analysis of the Role of Cortactin in Sealing Ring Formation and Bone Resorption

To address the possible role of cortactin in the maturation of actin aggregates to sealing ring, we knocked down or depleted cortactin using siRNA sequences. Untreated (Fig. 6*I*, *A*, *lane 1*) and scrambled RNAi (ScRNAi)-treated osteoclasts were used as controls. Osteoclasts were incubated with siRNA (*A*, *lanes 3* and *4*) or ScRNAi (*lane 2*) for 18–20 h at the indicated doses as described previously (7). A dose-dependent decrease in the cortactin level was observed in osteoclasts treated with siRNA to cortactin and incubated for 16–18 h at 37 °C (*A*, *lanes 3* and *4*). The decrease was maximal at 200 nM siRNA (~90–95%; *lane 4*) as compared with the levels of protein in ScRNAi-transfected osteoclasts (*A*, *lane 2*). The viability of osteoclasts was tested by a trypan blue exclusion test. Immunoblotting with a GAPDH antibody was used as a loading control (Fig. 6*I*, *B*).

After transfection with siRNA and ScRNAi for 18–20 h, osteoclasts were cultured on dentine slices for 10–12 h. Osteoclasts transfected with ScRNAi displayed mature sealing rings (Fig. 6*II*, *A* and *D*). Localization of cortactin (6*II*, *A*)

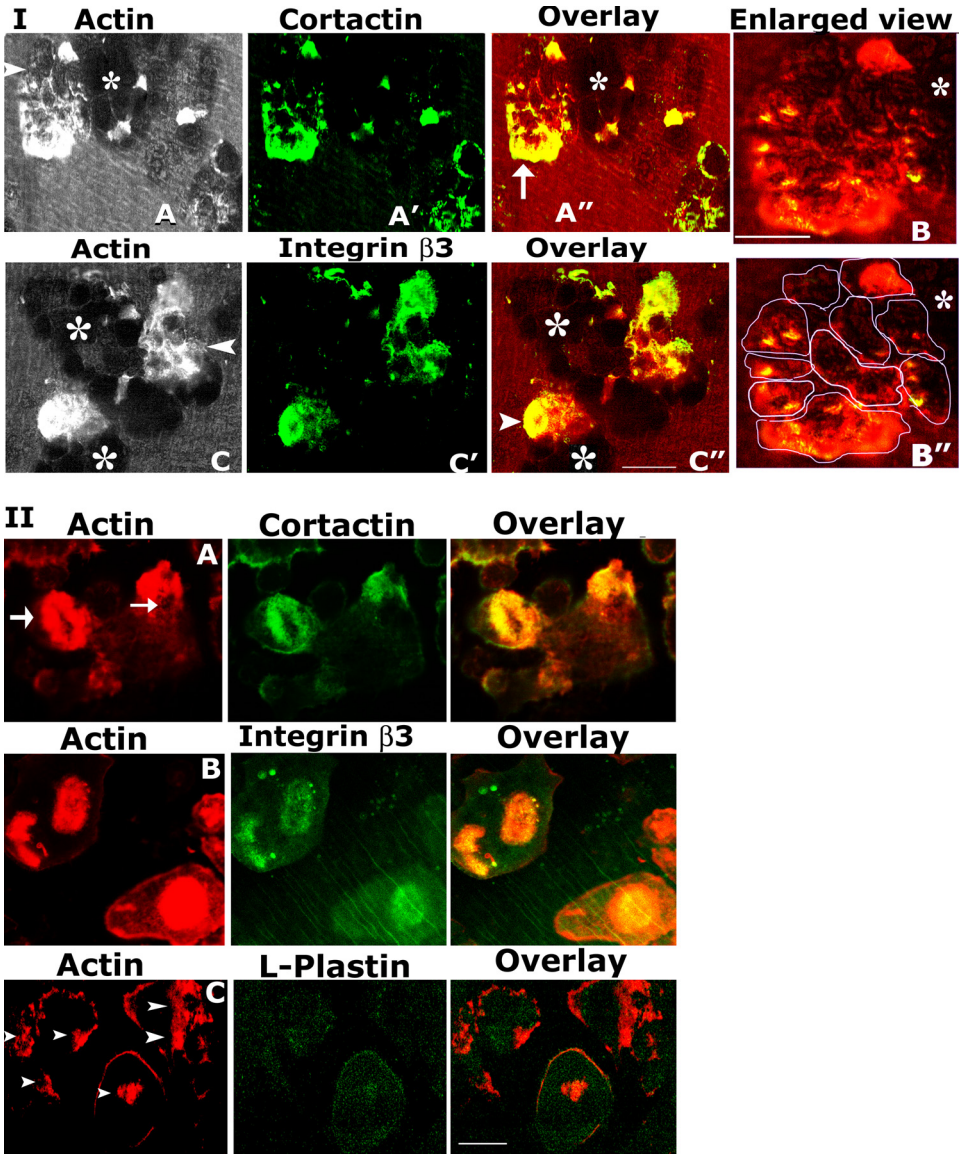

FIGURE 7. *I*, confocal analysis of localization of actin with cortactin and integrin β3. Osteoclasts cultured on dentine slices for 12–14 h were processed for double staining with actin/cortactin (*I*, *A* and *B*) and actin/integrin β3 (*C*). Confocal microscopic images of osteoclasts stained for actin (*A–C*, *red*), cortactin (*A′*, *green*), and integrin β3 (*C′*, *green*) are shown. *Yellow color* represents colocalization of cortactin and integrin β3 with actin (*overlay panels A″* and *C″*). A higher magnification view of the area indicated by an *arrow* in *A″* is shown in *B* and *B″*. More than eight actin rings (*outlined* in *B″*) were observed in this osteoclast. Resorption pits are indicated by *asterisks*, and an osteoclast that exhibits single or multiple sealing rings is indicated by an *arrowhead* (*A*, *C*, and *C″*). *Scale bars*, 10 μm (*B*) and 25 μm (C″). *II*, confocal analysis of localization of actin with cortactin, integrin β3, and L-plastin in osteoclasts treated with siRNA and ScRNAi to cortactin. Osteoclasts were treated with ScRNAi (*A*) and siRNA to cortactin (*B* and *C*). Confocal microscopic images of osteoclasts stained for actin (*A–C*, *red*), cortactin (*A*, *green*), integrin β3 (*B*, *green*), and L-plastin (*C*, *green*) are shown. *Yellow color* represents colocalization of cortactin and integrin β3 with actin (*overlay panels A* and *B*). *Scale bar*, 25 μm. The results represent one of the three separate experiments performed with three different osteoclast preparations.

and actin (*A′*) was observed in the sealing ring of resorbing osteoclasts. The *in vitro* bone resorption assay displayed an increase in the pit area or complexity with untreated and scrambled RNAi-treated osteoclasts (Fig. 6*III*, *A* and *B*). A significant decrease in the staining of cortactin was observed in a dose-dependent manner in siRNA to cortactin-treated cells (Fig. 6*II*, *B* and *C*). The effects of scrambled RNAi and siRNA on multiple osteoclasts are shown (Fig. 6*II*, *D* and *E*). Osteoclasts transfected with siRNA to cortactin displayed either small actin rings (indicated by *arrows* in Fig. 6*II*, *E* and *E′*) or actin aggregates (Fig. 6*II*, *B′* and *C′*; indicated by *asterisks* in *E*). A decrease in bone resorption *in vitro* was observed (Fig. 6*II*, *E″*) in a dose-dependent manner (Fig. 6*III*, *C* and *D*). The presence of actin aggregates and the failure of sealing ring formation in siRNA-treated cells suggest that cortactin-mediated actin polymerization is involved in the maturation of the sealing ring.

Localization of Integrin β3 in Sealing Ring

L-plastin phosphorylation has been shown to associate with integrin activation (47). Osteoclasts cultured on dentine slices for 12–14 h were processed for double staining with actin/cortactin (Fig. 7, *A* and *B*) and actin/integrin β3 (Fig. 7*C*). Diffuse colocalization of actin with cortactin (Fig. 7*A″*) and integrin (Fig. 7*C″*) was observed in resorbing osteoclasts. Osteoclasts are capable of organizing two to four sealing rings during bone resorption (Figs. 1 and 6) (11). We thought that a group or linear series of resorption pits were formed by sequential processes of resorption, motility, and adhesion of osteoclasts along the surface of dentine or bone. The results shown in Fig. 7*I* (*A″* and *C″*) also suggest that a multinucleated giant osteoclast can orchestrate sealing rings in greater number (*i.e.* 6–8 at a time) (Fig. 7*I*, *B*, *B″*, and *C″*), which leads to the formation of a group of resorption pits underneath the osteoclast (Fig. 7*I*, *A″* and *C″*). Osteoclasts exhibiting either single (Fig. 7*I*, *C″*, *arrowhead*) or multiple (Fig. 7*I*, *A″*, *B*, and *C″*) sealing or actin rings during bone resorption were observed. The osteoclast, which is indicated by an *arrow* (Fig. 7*I*, *A″*), is shown at higher magnification in Fig. 7*I*, *B* and *B″*. Colocalization of actin with cortactin was observed in patches in a confocal microscopy scan of the osteoclast taken at the level of dentine (Fig. 7*I*, *B* and *B″*). More than eight actin rings (outlined in Fig. 7*I*, *B″*) were observed in this osteoclast. The sealing rings formed were efficient and functional, which is recognized from the matching resorption pit underneath the osteoclast (indicated by an *asterisk* in Fig. 7*I*, *B*, *B″*, and *C″*).

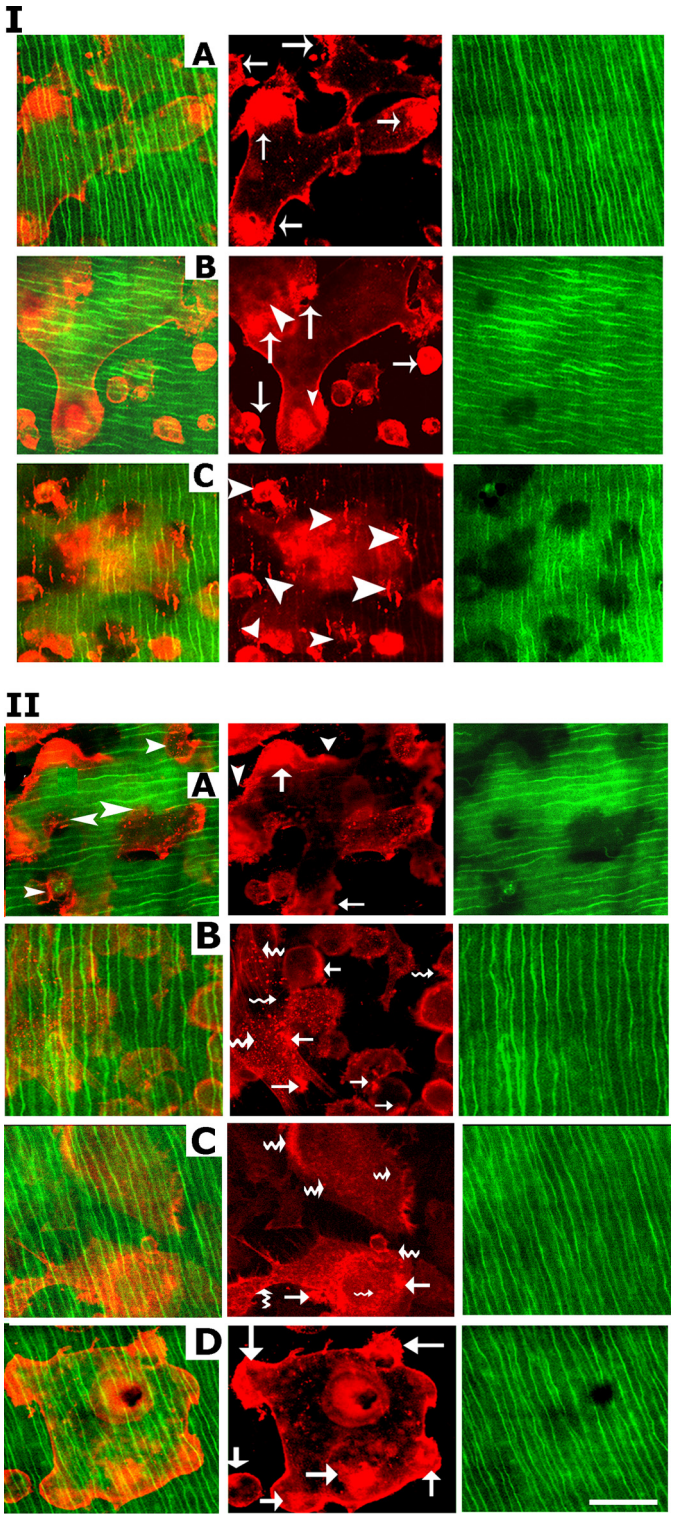

FIGURE 8. *I*, confocal analysis of time-dependent changes in actin organization and bone resorption in response to TNF-α. Osteoclasts plated on dentine slices were treated with TNF-α for 2–3 h (*A*), 8 h (*B*), and 12 h (*C*). Confocal microscopic images of osteoclasts stained for actin are shown. Distribution of actin (*red*) and scans of dentine slices (*green*) are shown separately. Several resorption pits were observed after incubation with TNF-α for 12–14 h. *II*, confocal analysis of the effects of various treatments on sealing ring formation and bone resorption. Osteoclasts were treated with a neutralizing antibody to TNF-α (*B*), Src (*C*), and αv inhibitor (*D*) in the presence of TNF-α. Osteoclasts treated together with a species-specific IgG and TNF-α were used as control (*A*) for neutralizing antibody to TNF-α antibody treatment (*B*). Sealing rings are indicated by *arrowheads* in *A*. Punctate podosome-like structures are indicated by *crooked arrows* in *B* and *C* (*red panel*). Actin patches (*B* and *C*, *red panel*) and aggregates are indicated by *arrows* (*D*, *red panel*). Bone resorption is considerably reduced in osteoclasts treated with a neutralizing antibody to TNF-α (*B*) and inhibitors to Src and αv (*C* and *D*) in the presence of TNF-α (*green panels*). *Scale bar*, 25 μM. The results represent one of the three separate experiments performed with three different osteoclast preparations.

The Effect of Cortactin Depletion on the Formation of Sealing Ring

After treating with ScRNAi (Fig. 7*II*, *A*) and siRNA (Fig. 7*II*, *B* and *C*) to cortactin for 18–20 h, osteoclasts were cultured on dentine slices for 8–12 h. Cells were double-stained for actin/cortactin, actin/integrin β3, and actin/L-plastin. Osteoclasts transfected with ScRNAi displayed colocalization of actin and cortactin in sealing rings (7*II*, *A*). As shown in Fig. 6, actin aggregates were found in osteoclasts transfected with siRNA to cortactin (Fig. 7*II*, *B* and *C*). These actin aggregates demonstrated colocalization of integrin β3 (Fig. 7*II*, *B*) but not L-plastin (Fig. 7*II*, *C*). L-plastin staining was observed throughout the osteoclasts but at a very minimal level. The reduced staining corresponds with the reduced L-plastin levels at 8–20 h in osteoclasts incubated with bone particles for 4–20 h (Fig. 3*B*). Failure of maturation of the sealing ring in cortactin-depleted osteoclasts (Fig. 6) despite the localization of integrin αv (data not shown) and β3 in actin aggregates (Fig. 7*II*, *B*) suggests that the maturation process is dependent on cortactin. Other actin-binding protein(s) could not recompense its role in the maturation process.

Analysis of Actin Distribution in Response to Treatment with TNF-α

Several studies report interesting outcomes for the role of TNF-α in osteoclast differentiation and function (24, 25, 39, 48, 49). Cyclical changes in L-plastin and cortactin protein levels were observed in a time-dependent manner (Fig. 4, *A* and *B*). Next, we proceeded to determine if TNF-α could reproduce the effects mediated by RANKL in the chronological processes of organization of the mature sealing ring. Therefore, osteoclast precursors were cultured on top of dentine slices and incubated for 2–3 h at 37 °C for adhesion. After adhesion for 2–3 h, cells were replaced with fresh medium containing TNF-α and M-CSF, and incubation at 37 °C was continued for 4, 8, and 12 h. Cells were fixed and stained with rhodamine-phalloidin to determine the distribution of actin. Consistent with previous studies (24), we have shown here that TNF-α has a role in osteoclast sealing ring formation during bone resorption. We have observed time- dependent changes in the organization of actin filaments. TNF-α treatment simulates the formation of actin aggregates at 3–4 h (Fig. 8*I*, *A*). Between 8 and 10 h, the size of actin aggregates increased in addition to the formation of some actin rings. Osteoclasts spread well and form multiple actin or sealing rings at 12–14 h (Fig. 8*I*, *C*). Actin rings (indicated by the *arrowheads* in Fig. 8*I*, *B* and *C*) formed at 8 h (*B*) and 12 h (*C*) are capable of resorbing bone, and pits were found underneath the sealing ring (*green panels* in *B* and *C*). TNF-α (Fig. 4*C*) reproduced the effects mediated by RANKL in changes in the levels of L-plastin and cortactin (Fig. 4*C*) as well as organization of the sealing ring in a time-dependent manner.

Studies with anti-TNF-α and anti-TNFR1 suggest that TNFR1 can elicit signals related to the formation of actin aggregates because osteoclasts treated with these antibodies failed to show changes in the levels of L-plastin (Fig. 4*C*, *lanes* 6 and 7). Therefore, to further elucidate the possible role of TNF-α signaling in osteoclast cytoskeletal reorganization during bone resorption, osteoclasts were treated with the neutralizing antibody to TNF-α (Fig. 8*II*, *B*), Src inhibitor (Fig. 8*II*, *C*), and αv inhibitor (Fig. 8*II*, *D*) plus TNF-α for 12–16 h. Osteoclasts treated with a species-specific non-immune IgG in the presence of TNF-α were used as a control (Fig. 8*II*, *A*) for the antibody treatment shown in Fig. 8*II*, *B*. Osteoclasts were stained for actin with rhodamine-phalloidin (Fig. 8*II*). Consistent with the observation shown in Fig. 8*I*, *C*, TNF-α not only increased the spreading of osteoclasts but also the formation of several sealing rings in one osteoclast. Nonspecific IgG had no effect on the changes elicited by TNF- α (Fig. 8*II*, *A*).

A neutralizing antibody to TNF-α, Src inhibitor, and αv inhibitor reduced the effects of TNF-α at different levels. These osteoclasts displayed a considerable decrease in bone resorption (Fig. 8*II*, *B–D*, *green panel*). Osteoclasts treated with a neutralizing antibody to TNF-α (Fig. 8*II*, *B*) and an Src inhibitor (8*II*, *C*) in the presence of TNF-α demonstrate comparable effects. Under both conditions, punctate and small patchy actin structures were observed in these osteoclasts (*B* and *C*). Punctate structures resemble podosomes and are distributed throughout the osteoclasts and at the periphery (8*II*, *B* and *C*; indicated by *crooked arrows*). Actin patch-like structures are smaller in size. Therefore, both podosome- and actin patch-like structures may compromise cell adhesion on bone but not actin aggregate or sealing ring formation. TNF-α signaling might be essential for the disassembly of podosomes and formation of actin aggregates. It is possible that Src may be part of a TNF-α-activated signaling pathway. In contrast, osteoclast treated with αv inhibitor exhibited actin aggregates in the presence of TNF-α and M-CSF. αv inhibitor indeed reduced the maturation of actin aggregates to the sealing ring. Therefore, bone resorption is considerably reduced in these osteoclasts (Fig. 8*II*, *D*, *green*). The presence of actin aggregates (8*II*, *D*, *red*; indicated by *arrows*) in these osteoclasts suggests that it occurs upstream and also independent of integrin signaling. Formation of actin aggregates in osteoclasts treated with a αv inhibitor suggests that the maturation of the sealing ring is under the aegis of integrin αvβ3 signaling.

DISCUSSION

There is a linear correlation between the size of the osteoclasts and the number of nucleus (50). The area of the resorption pit formed by each osteoclast can be correlated with the number of nuclei and size of the osteoclast. This is because those multinucleated giant osteoclasts can cover a large area on the bone and consequently form big resorption pits (51). Big osteoclasts make multiple contacts by membrane extension and demonstrated marginal or peripheral crawling, as shown in this paper (Figs. 1 and 5–8). Therefore, they are capable of forming multiple sealing rings, which resulted in the formation of multilocular pits (Figs. 4 and 6–8). Small osteoclasts are capable of making either simple (single) pits or contiguous pits linearly (Fig. 7*C*″, indicated by an *arrowhead*) (32). The latter is due to sequential events of cell adhesion, resorption, and migration of osteoclasts in one direction. It is not known whether an osteoclast can make multiple sealing rings during bone resorption *in vivo*. However, it is likely, based on time lapse live analyses performed by several investigators, including our own using various mineralized matrices, such as dentine (supplemental Fig. S1) and bone slices (52) as well as discs coated with apatite·collagen complexes (53, 54).

In an early study, osteoclasts have been shown to develop different patterns of contact characteristics, such as rings, crescents, and patches. Formation of these structures reflects the progress of the cell in the process of bone resorption. Osteoclasts are uniquely motile in that they continue to resorb bone beneath one area of the cell while another area is moving and reorganizing a sealing ring (55). Our study also shows that osteoclasts make actin aggregates or patches during the extension of the membrane. These secondary actin adhesive aggregates or patches confer extensive adherence and unique motile behavior as well as membrane extension (Figs. 7 and 8). These are consistent with the observations shown by others in the formation of actin-rich adhesion structures prior to the formation of the sealing ring (52). These actin aggregates may function as secondary adhesive structures and assist in the spreading of osteoclasts (Fig. 1, *A–C*). The spreading of osteoclasts with traction by the secondary actin adhesive structures increases the surface area. This may also possibly decrease the distance between osteoclasts and bone to facilitate proximity of ruffled border to bone. Actin aggregate formation seems to be necessary for the ensuing development of the sealing ring (Figs. 5–8) regardless of the number of sealing rings. Actin aggregates were 8–10-fold larger (Figs. 1 and 5–8) than podosome- or actin patch-like structures observed in osteoclasts treated with a neutralizing antibody to TNF-α (Fig. 8*II*, *B* and *C*). We consider that these actin aggregates or patches may be precursors for the sealing ring.

It is generally thought that the sealing ring is derived from the fusion of podosomes (14, 56, 57). However, several findings suggest that the sealing ring on bone has a different three-dimensional organization not derived from podosomes. The spatial arrangement of the presealing zone (referred to as actin aggregates) demonstrated neither clusters nor rosettes of podosomes. We found that osteoclasts plated on gelatin substrate (a non-mineralized matrix) organize either rosettes or clusters of podosomes at the migration front. These podosomes were capable of degrading the gelatin matrix because of the presence of MMP9 in these structures (36). Also, degradation of the matrix underneath the osteoclasts was not observed. These structures are different from typical podosome structures that are observed in osteoclasts during adhesion and migration (1, 36). Based on the time-dependent analysis (Fig. 5) and previous reports of others (53, 58), we suggest that sealing rings may not be the derivative of podosomes. We suggest this based on our previous observations in osteoclasts generated from gelsolin null ($Gsn^{-/-}$) mice. A dearth of gelsolin blocks podosome assembly and motility but not sealing ring formation and bone resorption (1). The resorbed areas by these osteoclasts are simple and non-contiguous due to the hypomotile nature of oste-

oclasts (1). Observations in $Gsn^{-/-}$ OCs also suggest that the organization of the sealing ring necessitates the role(s) of different actin-regulatory proteins.

We have observed time- dependent changes in the levels of L-plastin and cortactin in osteoclasts subjected to bone resorption (Figs. 2–4). It is interesting to speculate that actin aggregates are formed by L-plastin due to its actin bundling property (Fig. 5). This occurs at the early phase of bone resorption. Actin aggregates may function as an assembly center in the localization of integrin and other signaling molecules that are critical in the maturation of actin aggregates to functional sealing rings. L-plastin was described to be homologous with the F-actin-bundling protein fimbrin (59), and it is present in the podosomes of osteoclasts (2, 60). However, its function in osteoclasts is highly unknown. Analysis in L-plastin null osteoclasts ($LPL^{-/-}$) demonstrated normal osteoclast differentiation and peripheral podosomes. However, significant decreases in the formation of the adhesive contact region (actin aggregates) reduces not only the functional sealing ring formation but also the membrane extension or marginal unique motile quality (data not shown). Our results provide the first evidence of the role of L-plastin in the formation of actin aggregates in osteoclasts.

Cortactin is an important substrate for Src kinase (61). Cortactin has been implicated in osteoclast podosome assembly/disassembly and bone resorption (6, 10, 62, 64). siRNA to cortactin blocked sealing ring formation, but these osteoclasts displayed actin aggregates (Figs. 6 and 7*II*). Although siRNA to cortactin inhibits the maturation of the sealing ring, it had no effect on the function of L-plastin, formation of actin aggregates (Figs. 6 and 7*II*), and localization of integrin $\alpha v\beta 3$ (Fig. 7*II*, *B*). Taken together, these data suggest that cortactin-mediated actin polymerization occurs at the later stage of sealing ring formation. The roles of several signaling molecules and integrin signaling in the formation of the sealing ring are currently identified. However, the role of integrin signaling in the maturation of the sealing ring has not been studied well. Phosphorylation of L-plastin on serine residues is associated with the integrin activation (65). Localization of integrin $\alpha v\beta 3$ (Fig. 7, *I* and *II*) in the actin aggregates may play a role in the maturation of actin aggregates to the sealing ring.

Up-regulation of signaling proteins, such as c-Src, Rho, Rho kinase, and cortactin, was observed in osteoclasts subjected to bone resorption (Fig. 3, supplemental Fig. S2, and supplemental Table S1). Interestingly, osteoclasts subjected to the following treatments blocked maturation of the sealing ring and bone resorption but displayed actin aggregates. The treatments are: echistatin (66); bisphosphonates (31); αv inhibitor (Fig. 8); phenyl arsine oxide (an inhibitor to PTP-PEST) (10); and siRNA to cortactin (Fig. 6) (6), PTP-PEST, or WASP (7, 10). Consistent with our observations, WASP null osteoclasts also demonstrated actin patches and reduced bone resorption (8). Integrin $\beta 3$ (Fig. 7*II*), WASP, and Src localize to the actin aggregates of osteoclasts treated with siRNA to cortactin (Fig. 7*II*) or PTP-PEST (7) and bisphosphonates (10). The failure of formation of mature sealing ring in these osteoclasts suggests different levels of defective downstream integrin signaling mechanism. Cortactin integrates signals from Src kinase to form a trimolecular complex (cortactin·WASP·Arp2/3), which activates actin polymerization (67–69). Reducing the levels of either one of the proteins seems to have an impact on osteoclast bone resorption (8).

The comparable actin staining in osteoclasts treated with Src inhibitor and neutralizing antibody to TNF-α suggests that Src also functions (Fig. 8) at the early stage of sealing ring formation (*i.e.* organization of the presealing zone or actin aggregates) in a TNF-α-dependent manner. There is clear evidence that human and mouse TNF-α stimulated the expression of c-Src in osteoclasts (70). Furthermore, we have shown previously a diffuse distribution of actin in osteoclasts expressing kinase-defective (KD) Src in the presence of RANKL. Neither podosomes nor actin aggregates were found in these osteoclasts (7). These observations raise the following questions. Does TNF-α regulate disassembly or turnover of podosomes and RANKL regulate the assembly of actin aggregates in osteoclasts? Does Src have a role at the early and late phase of sealing ring formation? Activation of Src by different signaling pathway may lead to varied downstream activation mechanisms and functional outcomes at the early and late phase of the sealing ring. As suggested by others, TNF-α could synergize with RANKL to increase osteoclast activation to a large extent (24). It is possible that the TNF-α/RANKL pathway could occur at the initial phase of sealing ring formation followed by the activation of integrin $\alpha v\beta 3$ signaling toward the maturation phase of the sealing ring. The role of TNF-α and RANKL-mediated pathways and the exact step in which Src kinase fits in this pathway to regulate the formation of actin aggregates via L-plastin remain to be determined.

Inhibition of integrin $\alpha v\beta 3$ signaling with a αv inhibitor or knockdown of $\beta 3$ integrin with an siRNA (data not shown) had negligible effect on either the phosphorylation of L-plastin at the serine 9 residue or the formation of actin aggregates. Treatment of osteoclasts with a αv inhibitor did not block the localization of integrin in actin aggregates. However, localization of Src and cortactin in actin aggregates was blocked. Therefore, these osteoclasts demonstrated defective downstream signaling. Integrin expression and ligand binding affinity were not changed in $Src^{-/-}$ osteoclasts despite the consequences of defective downstream signaling (71). Integrin $\beta 3$ knock-out mice displayed an osteosclerotic phenotype, suggesting that osteoclast activity is not completely affected (72). However, targeted disruption of Src leads to the osteopetrotic phenotype due to a defect in the activity of osteoclasts (73). This possibly suggests a multiplicity of roles for Src at different levels in osteoclast function, including (*a*) assembly/disassembly of podosomes for adhesion and migration; (*b*) formation of actin aggregates, which function as a center for orchestrating integrin signaling; and (*c*) maturation of actin aggregates to fully functional sealing ring.

Bone consists of organic (collagen and a variety of non-collagenous proteins) and inorganic components. Surface microgeometry of implants plays a role in tissue/cell-implant surface interactions. However, our understanding of its effects at cellular levels or responses of bone cells to implants is incomplete. Podosomes were observed in cells plated on glass coverslips. Either actin aggregates or sealing rings were found in osteoclast

cultures on apatite crystals (53), dentine (10, 11), or human bone sections (data not shown). Formation of an actin-rich sealing ring may depend on minerals present in the bone. Therefore, osteoclasts were incubated with non-demineralized (native bone) and demineralized bone particles for 16–18 h. Live cell imaging at 4–6 h and 12 h demonstrated that osteoclasts migrated toward and adhered to the demineralized bone particles (supplemental Fig. S5*A*). However, the failure of changes in the levels of cortactin in SDS-PAGE analysis in lysates made from osteoclasts treated with demineralized bone particles suggests that bone particles having mineral a crystal structure are resorbable by osteoclasts and physiologically well suited for the signaling mechanism orchestrated by integrin $\alpha v\beta 3$ (supplemental Fig. S5*B*). Cortactin controls osteoclastic bone resorption by regulating actin organization (64) (Figs. 5–7). Osteoclasts are able to adhere (supplemental Fig. S5*A*) and resorb the organic phase of bone. It may occur by a process localized to the attachment site of osteoclasts by protease activity (74) independent of sealing zone formation.

Commercial cortical crushed bones have been used as allografts for several purposes, including filling of bones to evade bone defects. Demineralized freeze-dried bone allografts have been used extensively for periodontal therapy to induce bone formation in human extraction sockets. Bone formation is the principle process in peri-implant healing. This occurs by migration and localization of bone cells in the area of implants, differentiation of bone cells (osteoblasts and osteoclasts), and bone resorption followed by bone formation. Biopsies from six of the seven grafted sites were evaluated for new bone formation. Demineralized freeze-dried bone allograft sites revealed the presence of dead particles of demineralized freeze-dried bone allografts with no evidence of bone formation on the surfaces of the implanted particles and no evidence of osteoclastic resorption of the bone particles (63, 75). Our *in vitro* observations indeed suggest that the organic phase of the bone is essential for the recruitment of bone cells. However, mineralized matrix is required for the bone resorption function of osteoclasts. We suggest that graft materials with a combination of organic and inorganic components besides bone substitute material or biocompatible polymer may support good remodeling process.

CONCLUSIONS

Our aim is to dissect the molecular mechanisms behind the cyclical processes of sealing ring formation. Taken together, our results suggest that TNF-α, RANKL, and integrin $\alpha v\beta 3$-mediated pathways play roles in sealing ring formation and bone resorption. L-plastin has a role in the earliest stages of sealing ring formation. Phosphorylation of L-plastin and its activation occur independently of integrin $\alpha v\beta 3$ signaling (data not shown). Src kinase may play a role in the formation of actin aggregates through the TNF-α/RANKL pathway. The TNF-α/RANKL pathway could occur at the initial phase of sealing ring formation, subsequently followed by the activation of integrin $\alpha v\beta 3$ signaling toward the maturation phase of the sealing ring. Although integrin signaling has been shown to play a role in the formation of the sealing ring, its role in the maturation of actin aggregate to sealing ring has not yet been studied. The presence of actin aggregates in osteoclasts treated with αv inhibitor, siRNA to cortactin, Src inhibitor, and bisphosphonates (which block PTP-PEST and Rho GTPase activity) suggests that the formation of actin aggregates occurs independently of these molecules. Src kinase plays a crucial role at each level. A novel mechanistic link between plastin and cortactin localization and function exists in sealing ring formation. The formation of a spatially and dynamically regulated functional sealing ring and optimal bone resorptive capacity relies on the integrin-dependent pathway, which may involve the formation of the trimolecular complex consisting of cortactin·WASP·Arp2/3.

Acknowledgments—We thank Dr. Michael Rogers (Bone Research Group, University of Aberdeen, Aberdeen, UK) for bisphosphonates. Two-dimensional gel electrophoresis and mass spectrometry were performed at the core facility of the University of Maryland (Baltimore, MD), and we gratefully acknowledge the technical assistance provided by Dr. Nandakumar Madayiputhiya (Sigma).

REFERENCES

1. Chellaiah, M., Kizer, N., Silva, M., Alvarez, U., Kwiatkowski, D., and Hruska, K. A. (2000) *J. Cell Biol.* **148,** 665–678
2. Babb, S. G., Matsudaira, P., Sato, M., Correia, I., and Lim, S. S. (1997) *Cell Motil. Cytoskeleton* **37,** 308–325
3. Hurst, I. R., Zuo, J., Jiang, J., and Holliday, L. S. (2004) *J. Bone Miner. Res.* **19,** 499–506
4. McMichael, B. K., Kotadiya, P., Singh, T., Holliday, L. S., and Lee, B. S. (2006) *Bone* **39,** 694–705
5. Chellaiah, M. A. (2005) *J. Biol. Chem.* **280,** 32930–32943
6. Tehrani, S., Faccio, R., Chandrasekar, I., Ross, F. P., and Cooper, J. A. (2006) *Mol. Biol. Cell* **17,** 2882–2895
7. Chellaiah, M. A., Kuppuswamy, D., Lasky, L., and Linder, S. (2007) *J. Biol. Chem.* **282,** 10104–10116
8. Calle, Y., Jones, G. E., Jagger, C., Fuller, K., Blundell, M. P., Chow, J., Chambers, T., and Thrasher, A. J. (2004) *Blood* **103,** 3552–3561
9. Banin, S., Truong, O., Katz, D. R., Waterfield, M. D., Brickell, P. M., and Gout, I. (1996) *Curr. Biol.* **6,** 981–988
10. Chellaiah, M. A., and Schaller, M. D. (2009) *J. Cell. Physiol.* **220,** 382–393
11. Ma, T., Samanna, V., and Chellaiah, M. A. (2008) *J. Mol. Signal.* **3,** 4
12. Chellaiah, M., Fitzgerald, C., Alvarez, U., and Hruska, K. (1998) *J. Biol. Chem.* **273,** 11908–11916
13. Duong, L. T., Lakkakorpi, P. T., Nakamura, I., Machwate, M., Nagy, R. M., and Rodan, G. A. (1998) *J. Clin. Invest.* **102,** 881–892
14. Lakkakorpi, P. T., Nakamura, I., Nagy, R. M., Parsons, J. T., Rodan, G. A., and Duong, L. T. (1999) *J. Biol. Chem.* **274,** 4900–4907
15. Sanjay, A., Houghton, A., Neff, L., DiDomenico, E., Bardelay, C., Antoine, E., Levy, J., Gailit, J., Bowtell, D., Horne, W. C., and Baron, R. (2001) *J. Cell Biol.* **152,** 181–195
16. Tanaka, S., Amling, M., Neff, L., Peyman, A., Uhlmann, E., Levy, J. B., and Baron, R. (1996) *Nature* **383,** 528–531
17. Hartman, G. D., and Duggan, M. E. (2000) *Expert Opin. Investig. Drugs* **9,** 1281–1291
18. Miyazaki, T., Sanjay, A., Neff, L., Tanaka, S., Horne, W. C., and Baron, R. (2004) *J. Biol. Chem.* **279,** 17660–17666
19. Gupta, A., Lee, B. S., Khadeer, M. A., Tang, Z., Chellaiah, M., Abu-Amer, Y., Goldknopf, J., and Hruska, K. A. (2003) *J. Bone Miner. Res.* **18,** 669–685
20. Teitelbaum, S. L. (2007) *Am. J. Pathol.* **170,** 427–435
21. Carron, C. P., Meyer, D. M., Engleman, V. W., Rico, J. G., Ruminski, P. G., Ornberg, R. L., Westlin, W. F., and Nickols, G. A. (2000) *J. Endocrinol.* **165,** 587–598
22. Horton, M. A., Dorey, E. L., Nesbitt, S. A., Samanen, J., Ali, F. E., Stadel, J. M., Nichols, A., Greig, R., and Helfrich, M. H. (1993) *J. Bone Miner. Res.* **8,** 239–247
23. Duong, L. T., Lakkakorpi, P., Nakamura, I., and Rodan, G. A. (2000) *Matrix*

Biol. **19,** 97–105
24. Fuller, K., Murphy, C., Kirstein, B., Fox, S. W., and Chambers, T. J. (2002) *Endocrinology* **143,** 1108–1118
25. Kobayashi, K., Takahashi, N., Jimi, E., Udagawa, N., Takami, M., Kotake, S., Nakagawa, N., Kinosaki, M., Yamaguchi, K., Shima, N., Yasuda, H., Morinaga, T., Higashio, K., Martin, T. J., and Suda, T. (2000) *J. Exp. Med.* **191,** 275–286
26. Azuma, Y., Kaji, K., Katogi, R., Takeshita, S., and Kudo, A. (2000) *J. Biol. Chem.* **275,** 4858–4864
27. Kaji, K., Katogi, R., Azuma, Y., Naito, A., Inoue, J. I., and Kudo, A. (2001) *J. Bone Miner. Res.* **16,** 1593–1599
28. Lam, J., Takeshita, S., Barker, J. E., Kanagawa, O., Ross, F. P., and Teitelbaum, S. L. (2000) *J. Clin. Invest.* **106,** 1481–1488
29. Lam, J., Abu-Amer, Y., Nelson, C. A., Fremont, D. H., Ross, F. P., and Teitelbaum, S. L. (2002) *Ann. Rheum. Dis.* **61,** Suppl. 2, ii82–ii83
30. Chellaiah, M., Biswas, R., Yuen, D., Alvarez, U. M., and Hruska, K. (2001) *J. Biol. Chem.* **276,** 47434–47444
31. Samanna, V., Ma, T., Mak, T. W., Rogers, M., and Chellaiah, M. A. (2007) *J. Cell. Physiol.* **213,** 710–720
32. Chellaiah, M. A., Kizer, N., Biswas, R., Alvarez, U., Strauss-Schoenberger, J., Rifas, L., Rittling, S. R., Denhardt, D. T., and Hruska, K. A. (2003) *Mol. Biol. Cell* **14,** 173–189
33. Chellaiah, M., and Hruska, K. A. (1996) *Mol. Biol. Cell* **7,** 743–753
34. Samanna, V., Wei, H., Ego-Osuala, D., and Chellaiah, M. A. (2006) *Exp. Cell Res.* **312,** 2214–2230
35. Chellaiah, M. A., Biswas, R. S., Yuen, D., Alvarez, U. M., and Hruska, K. A. (2001) *J. Biol. Chem.* **276,** 47434–47444
36. Desai, B., Ma, T., and Chellaiah, M. A. (2008) *J. Biol. Chem.* **283,** 13856–13866
37. Gil-Henn, H., Destaing, O., Sims, N. A., Aoki, K., Alles, N., Neff, L., Sanjay, A., Bruzzaniti, A., De Camilli, P., Baron, R., and Schlessinger, J. (2007) *J. Cell Biol.* **178,** 1053–1064
38. Boyce, B. F., Yoneda, T., Lowe, C., Soriano, P., and Mundy, G. R. (1992) *J. Clin. Invest.* **90,** 1622–1627
39. Abu-Amer, Y., Ross, F. P., McHugh, K. P., Livolsi, A., Peyron, J. F., and Teitelbaum, S. L. (1998) *J. Biol. Chem.* **273,** 29417–29423
40. Atkins, G. J., Haynes, D. R., Graves, S. E., Evdokiou, A., Hay, S., Bouralexis, S., and Findlay, D. M. (2000) *J. Bone Miner. Res.* **15,** 640–649
41. Kudo, O., Fujikawa, Y., Itonaga, I., Sabokbar, A., Torisu, T., and Athanasou, N. A. (2002) *J. Pathol.* **198,** 220–227
42. Boyce, B. F., Li, P., Yao, Z., Zhang, Q., Badell, I. R., Schwarz, E. M., O'Keefe, R. J., and Xing, L. (2005) *Keio J. Med.* **54,** 127–131
43. Murakami, H., Takahashi, N., Sasaki, T., Udagawa, N., Tanaka, S., Nakamura, I., Zhang, D., Barbier, A., and Suda, T. (1995) *Bone* **17,** 137–144
44. Rogers, M. J., Gordon, S., Benford, H. L., Coxon, F. P., Luckman, S. P., Monkkonen, J., and Frith, J. C. (2000) *Cancer* **88,** 2961–2978
45. Rogers, M. J. (2003) *Curr. Pharm. Des.* **9,** 2643–2658
46. Mundy, G. (2001) *Semin. Oncol.* **28,** 2–8
47. Jones, S. L., Wang, J., Turck, C. W., and Brown, E. J. (1998) *Proc. Natl. Acad. Sci. U.S.A.* **95,** 9331–9336
48. Horowitz, M. C. (1993) *Science* **260,** 626–627
49. Pacifici, R. (1996) *J. Bone Miner. Res.* **11,** 1043–1051
50. Piper, K., Boyde, A., and Jones, S. J. (1995) *Calcif. Tissue Int.* **56,** 382–389
51. Boissy, P., Saltel, F., Bouniol, C., Jurdic, P., and Machuca-Gayet, I. (2002) *Endocrinology* **143,** 1913–1921
52. Luxenburg, C., Geblinger, D., Klein, E., Anderson, K., Hanein, D., Geiger, B., and Addadi, L. (2007) *PLoS ONE* **2,** e179
53. Saltel, F., Destaing, O., Bard, F., Eichert, D., and Jurdic, P. (2004) *Mol. Biol. Cell* **15,** 5231–5241
54. Destaing, O., Saltel, F., Geminard, J. C., Jurdic, P., and Bard, F. A. (2003) *Mol. Biol. Cell* **14,** 407–416
55. Taylor, M. L., Boyde, A., and Jones, S. J. (1989) *Anat. Embryol.* **180,** 427–435
56. Teti, A., Marchisio, P. C., and Zallone, A. Z. (1991) *Am. J. Physiol.* **261,** C1–C7
57. Lakkakorpi, P. T., and Väänänen, H. K. (1991) *J. Bone Miner. Res.* **6,** 817–826
58. Jurdic, P., Saltel, F., Chabadel, A., and Destaing, O. (2006) *Eur. J. Cell Biol.* **85,** 195–202
59. Nakano, K., Satoh, K., Morimatsu, A., Ohnuma, M., and Mabuchi, I. (2001) *Mol. Biol. Cell* **12,** 3515–3526
60. Marchisio, P. C., Cirillo, D., Naldini, L., Primavera, M. V., Teti, A., and Zambonin-Zallone, A. (1984) *J. Cell Biol.* **99,** 1696–1705
61. Wu, H., and Parsons, J. T. (1993) *J. Cell Biol.* **120,** 1417–1426
62. Luxenburg, C., Parsons, J. T., Addadi, L., and Geiger, B. (2006) *J. Cell Sci.* **119,** 4878–4888
63. Becker, W., Urist, M. R., Tucker, L. M., Becker, B. E., and Ochsenbein, C. (1995) *J. Periodontol.* **66,** 822–828
64. Matsubara, T., Myoui, A., Ikeda, F., Hata, K., Yoshikawa, H., Nishimura, R., and Yoneda, T. (2006) *J. Bone Miner. Metab.* **24,** 368–372
65. Chen, H., Mocsai, A., Zhang, H., Ding, R. X., Morisaki, J. H., White, M., Rothfork, J. M., Heiser, P., Colucci-Guyon, E., Lowell, C. A., Gresham, H. D., Allen, P. M., and Brown, E. J. (2003) *Immunity* **19,** 95–104
66. Nakamura, I., Pilkington, M. F., Lakkakorpi, P. T., Lipfert, L., Sims, S. M., Dixon, S. J., Rodan, G. A., and Duong, L. T. (1999) *J. Cell Sci.* **112,** 3985–3993
67. Weaver, A. M., Karginov, A. V., Kinley, A. W., Weed, S. A., Li, Y., Parsons, J. T., and Cooper, J. A. (2001) *Curr. Biol.* **11,** 370–374
68. Tehrani, S., Tomasevic, N., Weed, S., Sakowicz, R., and Cooper, J. A. (2007) *Proc. Natl. Acad. Sci. U.S.A.* **104,** 11933–11938
69. Uruno, T., Liu, J., Li, Y., Smith, N., and Zhan, X. (2003) *J. Biol. Chem.* **278,** 26086–26093
70. Abu-Amer, Y., Ross, F. P., Edwards, J., and Teitelbaum, S. L. (1997) *J. Clin. Invest.* **100,** 1557–1565
71. Lakkakorpi, P. T., Nakamura, I., Young, M., Lipfert, L., Rodan, G. A., and Duong, L. T. (2001) *J. Cell Sci.* **114,** 149–160
72. McHugh, K. P., Hodivala-Dilke, K., Zheng, M. H., Namba, N., Lam, J., Novack, D., Feng, X., Ross, F. P., Hynes, R. O., and Teitelbaum, S. L. (2000) *J. Clin. Invest.* **105,** 433–440
73. Soriano, P., Montgomery, C., Geske, R., and Bradley, A. (1991) *Cell* **64,** 693–702
74. Blair, H. C., Kahn, A. J., Crouch, E. C., Jeffrey, J. J., and Teitelbaum, S. L. (1986) *J. Cell Biol.* **102,** 1164–1172
75. Schwartz, Z., Somers, A., Mellonig, J. T., Carnes, D. L., Jr., Wozney, J. M., Dean, D. D., Cochran, D. L., and Boyan, B. D. (1998) *J. Periodontol.* **69,** 1337–1345

SUPPLEMENTAL DATA

EXPERIMENTAL PROCEDURES

Two dimensional gel electrophoresis (2DGE) —About 300-500 μg protein was used for 2DGE. The 300 microgram of soluble protein mixture was initially rehydrated using 4-7 pI IPG strip (GE health care, USA) in rehydration solution with a composition of 8M urea, 4% CHAPS, 7mg DTT per 2.5 ml of rehydration buffer with 2% 4-7 IPG buffer (GE healthcare, USA). The rehydrated IPG strips were subjected to isoelectric focusing employing Electrophoretic IQ (Proteome system, USA) with an initial gradient voltage accumulation (10000V) in 8 hours followed by 16 hours holding at 10000V. The focused strips were used for 2DGE employing Electrophoretic IQ gel running apparatus (Proteome system USA) at a constant current of 30mA/gel for 120 min. The gels were stained with silver stain (Invitrogen USA). For visualization of protein, images were captured using Alpha Innotech image scanner (Alpha Innotech Corporation, USA). Global protein expression differences of the treated and untreated sample gels were compared using Z3 image analysis software (Compiegne, Israel).

Mass spectrometry— The selected spots/bands from the gels were initially trypsinized overnight at 37^0C using standard protocol after DDT reduction and Iodoacetamide alkylation. LC- MS analysis of tryptic peptides derived from protein samples was performed on Thermo finnigan LCQ XL mass spectrometer (Thermo Finnigan USA) which was connected to nanospray ionizer. The Surveyor chromatographic system with auto sampler (Thermo Finnigan, USA) was used for peptide separation. The LC system was connected to 10.5 cm fused silica reverse phase C18 column (Pico frit column, New Objective, USA). The peptides were separated during 90 minute linear gradient of 5-90% acetonitrile/water mixture, containing 0.1% formic acid at a flow rate of 300 nanolitre/min. The spectrums were accumulated and the acquired MS scans were searched against the mouse protein data base (IPI) using SORCERER search algorithm. The best hit was selected based on probability / percent of coverage and number of peptides.

Expression of GFP actin in osteoclasts and confocal microcopy analysis of localization of G-actin in live cells— Osteoclasts were transfected with human ß-actin containing an NH_2-terminal EGFP vector (Clonetech) using MIRUS reagent (Cat. No. MIR 2804**).** Expression of GFP-actin was confirmed at 10-12 h after transfection with an inverted microscope. Dentine slices were added to osteoclast cultures and images were acquired at 2-3h (Figure S3-A), 4-6h (S3-B), and 10-12h (3S-C) with a 1.4 NA Plan Apo 63x objective (Bio-Rad confocal microscopy). GFP was excited using a 488-nm laser line.

Real-time RT-PCR Analysis— Total RNA was extracted from osteoclast treated with bone for different time periods using Qiagen RNeasy mini kit protocol with the DNase digest (Qiagen). Reverse transcription reaction was performed in a 20μl-reaction volume with 1 μg of total RNA by following the instructions provided by the manufacturer (Invitrogen, Carlsbad, CA). The cDNA was stored at -20^0C until further use. For real time PCR, primers were designed by Primer Express software (Applied Biosystems Group). A total of 15 primer pairs (Table S2) were designed with amplification product length of 100–200 bp and annealing temperature of ~60 °C. 18s rRNA and GAPDH were used for normalization. About 600-900nM of each primer was used. Each reaction was performed in duplicates or triplicates in 25 μl volume in 96-well plates with a SYBR green reaction mix (Applied Biosystems Group) in an ABI 7000HT thermocycler (2 min at 50 °C, 10 min at 95 °C and 40 cycles of 15 s at 94 °C and 1 min at 60 °C). The expression was calculated relative to that of untreated control cells and normalized for 18S rRNA measured under the same conditions with Taq Man ribosomal RNA

control primers (Applied Biosystems/Roche, Branchburg, NJ), using the $2^{-}\Delta\Delta^{CT}$ method {Livak, 2001 6908 /id}.

RESULTS

Analysis of time-dependent changes in actin organization in osteoclasts subjected to migration towards dentine slices— Depending on the substratum upon which the osteoclasts are spread, there are two different structures of actin known as podosomes and the sealing zone. To understand the specific properties and relationship of podosomes and the sealing zone, we used live-cell imaging of cultured osteoclasts. Osteoclasts migrated towards dentine particles (Figure S1, indicated by arrow heads in A and C). Osteoclasts attached to the edges of dentine particles at 2-3h (A) and at this time, punctate distribution of actin was observed in the cytoplasm (Figure S3A and A'). Organization of actin-rich basolateral membrane-like structure occurs right opposite to the attachment zone to bone (indicated by asterisks in A'). At 4-6h, punctate actin structures were converted into peripheral plasma membrane-like structure (Figure S3, B). Actin aggregate (indicated by a wavy arrow in B') was observed at the attachment site to bone (B and B'). We believe that the actin aggregate is a precursor for a sealing ring (SR). At 10-12h (C), maturation of this actin aggregate into sealing ring (SR in C') was observed. Resorption pit (#2 in C") was found underside of the sealing ring (C). Two resorption pits were found adjacent to each other (#1 and #2 in panel C"). Single osteoclast is capable of forming multiple sealing rings during bone resorption (Fig.1B and C and ref. {Ma, 2008 7106 /id}). Extension of osteoclast membrane near resorption pit #1 suggests that both pits may perhaps be generated by the same osteoclast but at different time. It is also possible that the actin clumps observed near the resorption pit (#1 in C'') may be part of the disassembled sealing ring (DSR in C').

Analysis of cell lysates by two dimensional gel electrophoresis— To analyze the expression profile of proteins, we have first performed two-dimensional (2-D) gel electrophoresis (GE) using lysates (500μg) made from osteoclasts treated with (+) or without (-) bone particles (Figure S2). A representative 2-D gel stained with silver stain is shown in this figure. Gels were scanned using the image processing software (Z3, Compugen) to determine expression differences between the same spot of different gels. Approximately 200-250 protein spots could be detected in the 2D gels (Fig.5). The molecular masses of the intracellular proteins were distributed in the range of 25 kDa–150 kDa and isoelectric points of 4.0–7.0. About 18 unique, 12 down-regulated and 21 up-regulated spots were identified by Z3 analysis. Spots that show significant changes are indicated in the figure. Some of the proteins that are indicated by circles in untreated osteoclasts are down-regulated in osteoclasts treated with bone particles (B). A few of the up-regulated proteins are indicated by arrows in B.

Mass spectrometry analysis of protein spots after digestion with trypsin— The protein spots that demonstrated a significant change ($p<0.001$) in abundance between the protein fractions of osteoclasts untreated (-) and treated (+) with bone were selected for further characterization using mass spectrometry (MS). For example, spots (# 1 and 2 in Figure S1) were physically cut out from the gel and digested with trypsin to analyze by MS. A representative mass spectrum of one of the peptides (FSLVGIAGQDLNEGNR-highlighted in green) is provided (Figure S3). Trace yielded about 17 matching peptide masses, representing about 30-35% coverage for L-plastin. Peptide sequences identified in MS are highlighted in red (Figure S3). Similarly, trace yielded about 22 matching peptide masses, representing about 22-28% coverage for cortactin (data not shown). Peptides corresponding to proteins

such as, c-Src, gelsolin, vimentin, Arp 2, gCap39, actin, fyn, vacuolar H+ATPase B2, Cathepsin D were also identified in MS. A list is provided in the as Table S1**.**

Real time RT-PCR analysis— Observations from several laboratories including our own demonstrated that several signaling molecules are involved in the reorganization of actin cytoskeleton during migration and bone resoprtion To investigate further we quantitated the mRNAs using real-time PCR analysis (Figure S4). Thirteen genes were analyzed from the list of genes shown in Table S2. We determined the time course of bone particles effect on gene expression for four different time points (Figure S4). Although there was a decrease in L-plastin protein at 18-20h (Figures 3 and S1), a significant increase in mRNA (2-3 fold) was observed in real time RT-PCR analysis. The expression level of L-plastin did not change to a great extent at 4h, 8h, and 12h. There was a significant increase in the expression of Src and Rho GTPase was observed at all four time points tested. However, expression of cortactin, integrin beta 3 and Rho kinase was increased at 4h and 18h but decreased to either control level (cortactin) or below control level (beta 3 and Rho kinase) at 8 and 12 h. Addition of bone for 4-18h had no effect on the expression levels of WASP, Rho GAP, PYK2, Arp3, and alpha v. A time dependent increase in the expression of gelsolin was observed at 8, 12, and 18h.

We have shown in real time RT-PCR analysis that there are no changes in expression of L-plastin mRNA level during incubation for 4, 8, and 12h and an increase was observed at 18h. We hypothesized that the expression levels of L-plastin protein may be gradually reduced from 4-18h and increased after 18h. Therefore, we analyzed the L-Plastin protein levels as shown below. Changes in the RNA levels correspond with the protein levels shown in Figure 3. It is possible that the cyclical changes in the RNA/protein levels correspond with the formation of actin aggregates. Mass spectrometry and real time analyses revealed some of the key proteins involved in osteoclast bone resorption

Analysis of the effects of mineralized and demineralized bone particles on osteoclast function— Next, we have determined the effects of demineralized bone particles on osteoclasts migration and adhesion and changes in the protein levels (Figure S5) Bone particles from the long bone of mice were treated with 14% EDAT for two weeks and the demineralized bone particles (DMBP) were extensively with sterile PBS and pH was normalized to 7.2 prior to adding to osteoclasts. The texture of DMBPs was different from mineralized particles. DMBPs were inseparable and slimy in the culture medium. It is less dense (i.e. noticeably semi-transparent) and more fibrous under microscope (Figure S5). Upon incubation for 2-3h at 37^0C, the demineralized bone particles were found surrounded and adhered by osteoclasts. Migration of osteoclasts towards the particles was observed (Figure S5). Lysates made from osteoclasts treated with demineralized and mineralized bone materials for 16-18h were subjected to SDS-PAGE. Similar decrease in the levels of L-plastin and increase in cortactin was observed in osteoclasts treated with bone particles (Figure S5B, lane 2). Although a decrease in L-plastin level was observed in osteoclasts treated with DMBPs, cortactin level was either remained the same or decreased (lane 3) below control levels in these osteoclasts (lane 1). This suggests that activation of cortactin by integrin occurs during bone resorption in the presence of mineralized matrix which may not be necessary for the activity of L-plastin.

FIGURE LEGENDS

FIGURE S1. **Analysis of changes in the organization of GFP-labeled actin in osteoclasts incubated with dentine slices in vivo.** Osteoclasts expressing were added with dentine slices. Cells migrating towards and attached to dentine slices were visualized at 2-4h (A), 4-6h (B), and 10-12h (C). Migrating osteoclasts which express GFP-actin are indicated by arrow heads (A and C). The dentine is shown in red (pseudocolor) by the reflected light (A"-C"). Osteoclasts expressing actin protein is shown in green (A'-C'). Overlay images (A-C) show osteoclasts expressing GFP-actin (green) and bone (red). Two resorption pits were found adjacent to each other (indicated as 1 and 2 in C"). Wavy arrow points to actin aggregate. Asterisks indicate organization of a membrane-like structure opposite to the adhesion zone to bone. DSR-Disassembled sealing ring; SR- Sealing ring.

FIGURE S2. **Two dimensional electrophoresis (2DGE) of lysates made from OCs treated with (+) and without (-) bone for 16-18h.** Circles in Figure A indicate the proteins that are down regulated in OCs treated with bone (B). Upregulated proteins are indicated by arrows in osteoclasts treated with bone (+) (B). About 18 unique, 12 down regulated and 21 up regulated spots were identified by Z3 analysis. The protein spots that demonstrated a significant change ($p<0.001$) in abundance between the protein fractions of untreated and treated osteoclasts were selected for further characterization using mass spectrometry. Those proteins are indicated with numbers (1 and 2) in panels A and B (1' and 2'). A significant increase in cortactin (1 and 1') and decrease in L-plastin (2 and 2') level was observed in osteoclasts treated with bone (+ bone in panel C).

FIGURE S3. **Mass spectrometry and protein analysis. A.** Tryptic peptides of L-plastin found in mass spectrometry are shown in red. **B.** A representative mass spectrum of one of the peptides (**FSLVGIAGQDLNEGNR**-highlighted in green in A) is provided in the graph.

Table S1: Mass spectrometry results from osteoclasts subjected to bone resorption in the presence of bone particles are provided.

FIGURE S4. **Real-time quantitative PCR analysis.** TABLE S2: Primer used for real time PCR are provided. Primers were designed using Primer Express software (Applied Biosystems Group). Graph: mRNA expression of indicated genes in osteoclasts treated with bone at the indicated time (see insert) is provided. Untreated osteoclasts were used as controls. Results are reported as fold change in mRNA expression normalized to 18S ribosomal RNA and relative to control untreated RNA. Data shown are mean±SEM of three independent osteoclast preparations and experiments. ***$p<0.001$, **$p<0.01$,*$p<0.05$ vs. control osteoclasts untreated with bone.

TABLE S2: Real time PCR analysis: Primers used for the indicated proteins are provided.

FIGURE S5. **Analysis of the expression profile of proteins and cell shape changes in osteoclasts treated with demineralized bone particles (DMBPs).** Treatment of osteoclasts with bone particles were performed as described in the Methods section. DMBPs were added to mature osteoclast cultures (100μg/well in a six well cell culture plate). Pictures were taken in an inverted phase contrast microscope. Migration and adhesion of osteoclasts were observed at 2-3h (A). About ~300μg of lysate proteins made from osteoclasts incubated with normal (B, lane 2)

and DMBPs (lane 3) for 16-18h were subjected to 10% SDS-PAGE analysis. Cortactin (Cttn) and L-plastin (LPL) are indicated by arrows.

Figure S1

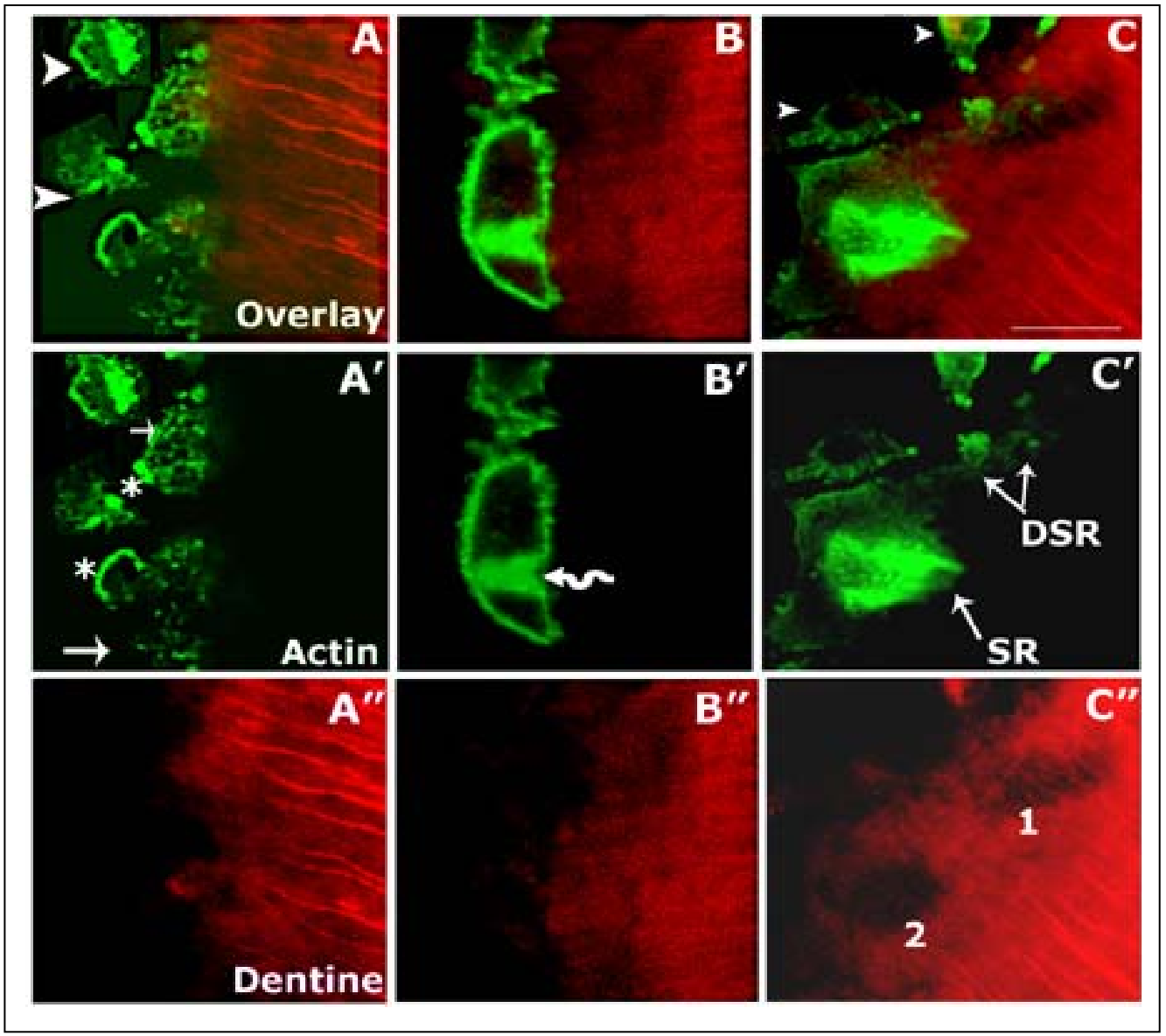

Figure S2

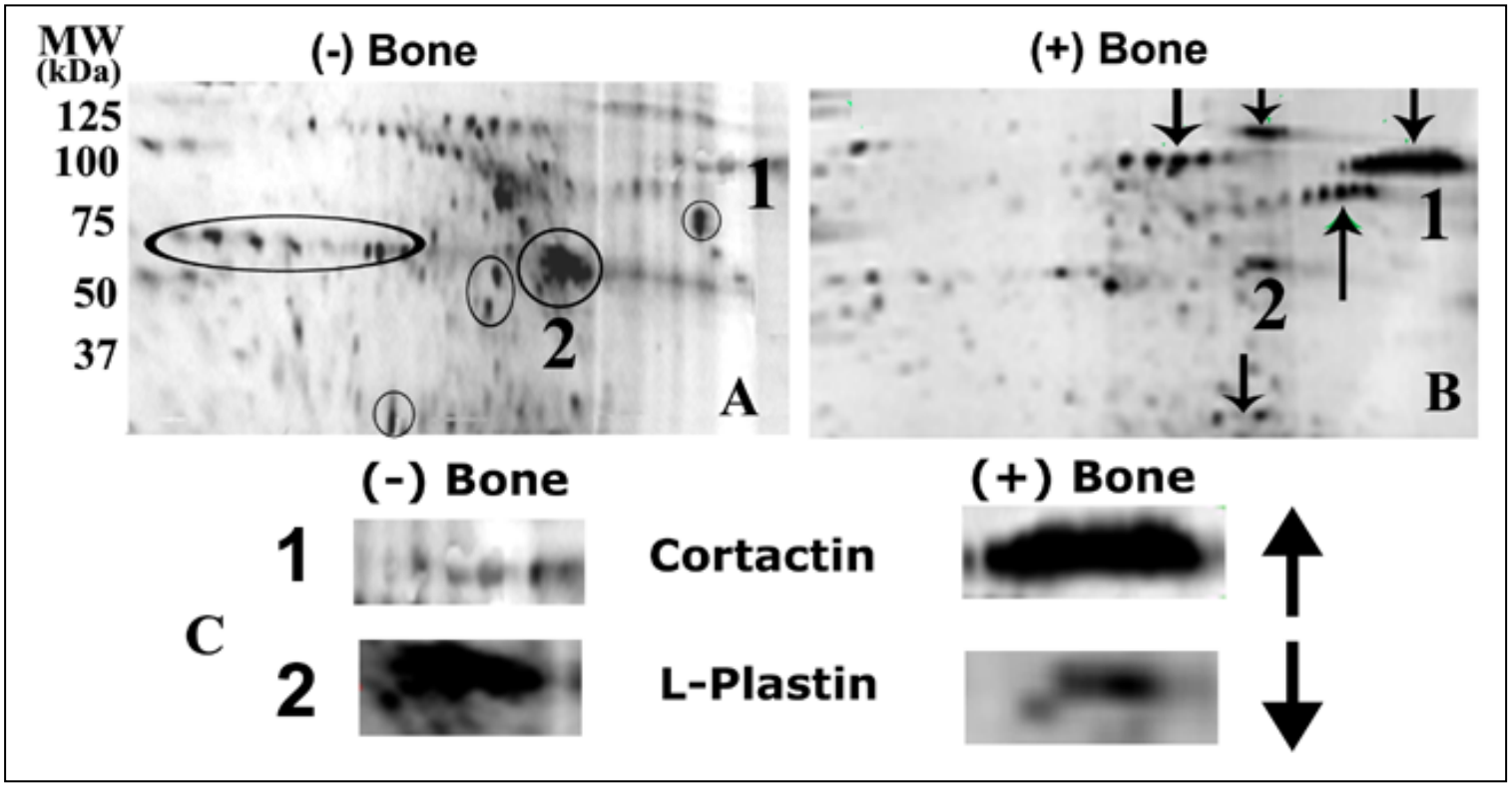

Figure S3

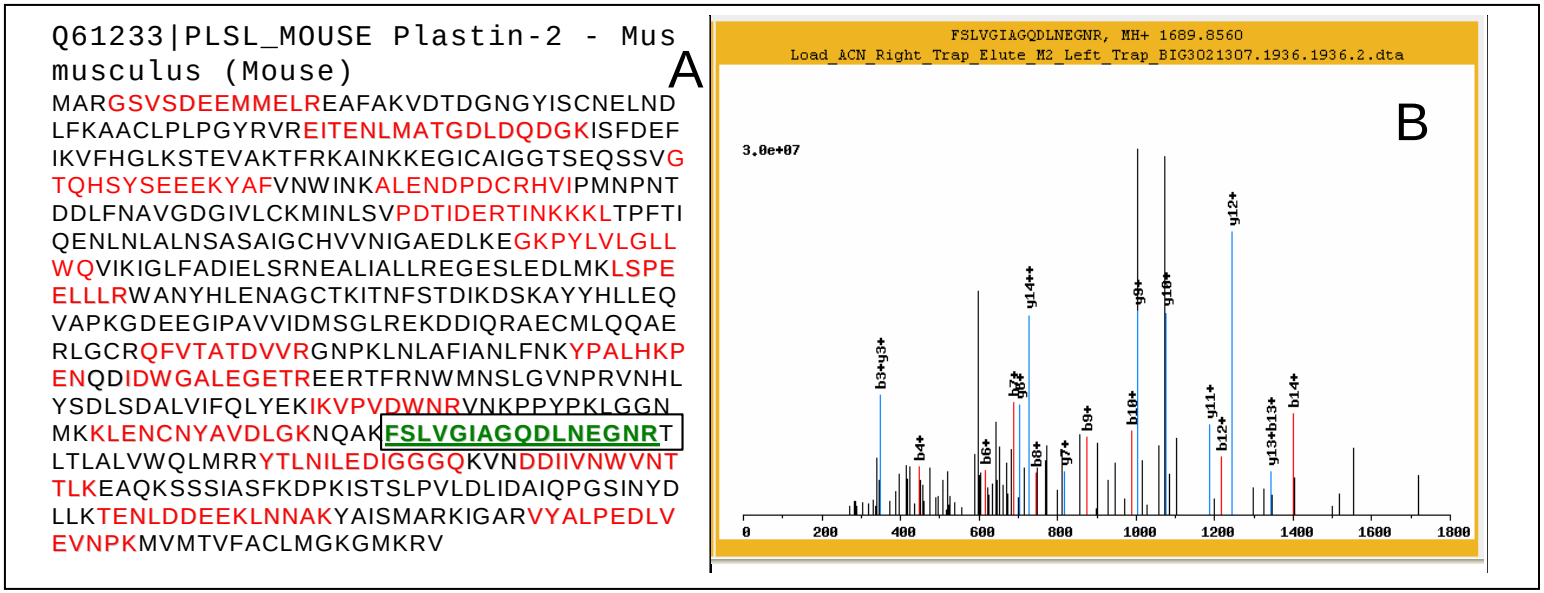

Table S1

Protein Name	Accession number	Protein probability	Sorcerer	
			percent coverage	Number peptides
(-) Bone				
Isoform C of Lamin-A\C,Isoform A of Lamin-A\C	NP_001002011.1	1	2.4	3
Plastin-2 or L-plastin	NP_032905.2	1	30	17
Transketolase	NP_033414.1	1	2.9	1
Myosin-4	NP_034988.2	1	1.3	2
D-amino acid oxidase 1,D-amino-acid oxidase	NP_034148.2	1	3.2	1
Zfp473 protein,MKIAA1141 protein (Fragment),Zinc finger protein 473 homolog	NP_848849.2	0.98	1.2	31
diacylglycerol kinase, iota isoform 1	NP_001074675.1	0.9	1.3	3
Isoform 2 of Teneurin-3	NP_035986.2	0.78	0.8	2
Filamin-B	NP_598841.1	0.74	0.6	3
Isoform 2 of E3 ubiquitin ligase TRIAD3	NP_542128.2	0.69	1.5	1
LYR motif-containing protein 1	NP_083886.1	0.67	7.4	3
mannose-6-phosphate receptor binding protein 1	NP_080112.1	0.67	23.8	3
Probable ATP-dependent RNA helicase DDX28	NP_082314.1	0.63	1.7	1
Nuclear RNA export factor 7	NP_570958.1	0.57	2.2	3
toll-interleukin 1 receptor (TIR) domain- containing adaptor protein(blast)	NP_473437.1	0.56	6.2	1
leukotriene A4 hydrolase	NP_032543.2	0.56	4.6	1
Hira protein	NP_034565.2	0.53	2.4	1
Rab proteins geranylgeranyltransferase component A 1	XP_996584.1	0.49	5.7	3
Myosin-11	NP_038635.1	0.49	1.1	2
Limb bud and heart	XP_984828.1	0.49	15.2	1
CCR4-NOT transcription complex, subunit 10	NP_058573.2	0.48	1.5	1
sideroflexin 5	NP_848754.1	0.48	7.2	1
Isoform 3 of ULK3	XP_930106.2	0.46	5.4	1
IFN-response-binding factor 1	P22560	0.44	3.5	1
zinc finger protein 507	XP_001002219.1	0.41	1.5	1
Ankyrin repeat and BTB\POZ domain-containing protein 2	NP_849221.2	0.4	1.2	1
Tcte-1 peptide	NP_038716.2	0.4	2.2	1
WAS protein family, member 2 (blast)	NP_700472.1	0.39	1.2	1
Polycystic kidney disease 1 protein	NP_038658.2	0.38	0.3	1
DEAD (Asp-Glu-Ala-Asp) box polypeptide 21,Nucleolar RNA	NP_080814.1	0.37	1.8	1

helicase 2				
P47 protein (blast)	XP_977730.1	0.36	3.7	1
heterogeneous nuclear ribonucleoprotein H3	NP_001073293.1	0.34	3.9	1
Fanconi anemia, complementation group E	XP_996088.1	0.33	2.7	1
Isoform 3 of Phosphoinositide 3-kinase regulatory subunit 6	NP_001004435.1	0.32	3.9	1
Probable G-protein coupled receptor 55	NP_001028462.2	0.32	3	2
radial spokehead-like 2a (blast)	NP_080065.3	0.32	6.4	1
Salivary glue protein Sgs-4 precursor	XP_920575.1	0.32	0.9	3
STYK1	NP_766479.1	0.32	2.9	3
ezrin-binding partner PACE-1	NP_083052.1	0.32	2	1
zinc finger protein 62 (blast)	NP_001020017.1	0.3	1.6	1
protein phosphatase 1A, magnesium dependent (blast)	NP_067366.1	0.3	3.2	1
Angiotensin-converting enzyme, somatic isoform precursor	XP_110936.5	0.29	0.9	2
synaptosomal-associated protein 23 (blast)	NP_033248.1	0.28	5	1
ADAM 18 precursor	XP_988097.1	0.28	1.3	2
BCL2-like 12 (proline rich) (blast)	NP_083686.1	0.28	3.5	1
Isoform 1 of von Willebrand factor precursor	NP_073725.2	0.27	0.4	4
VIP36-like protein precursor	XP_892360.1	0.26	3.5	1
Hypothetical protein Golgin-160-like	XP_139904.5	0.24	2.3	1
Zinc finger CCHC domain-containing protein 10	NP_080755.2	0.24	3.9	1
ubiquitin specific protease 31	XP_357781.3	0.24	1.3	1
Beta-1,4 N-acetylgalactosaminyltransferase 2	NP_032107.1	0.24	3.1	1
cortactin(blast)	NP_031829.2	0.23	3	7
Mannose-6-phosphate receptor-binding protein 1	NP_080112.1	0.23	2.5	1
serine (or cysteine) peptidase inhibitor, clade A, member 3H	NP_001030042.2	0.23	2.2	1
Transcriptional intermediary factor 1 delta	NP_862901.2	0.23	1.5	1
Ras and Rab interactor 2 (blast)	NP_083000.4	0.22	0.8	1
growth factor, erv1	NP_075527.2	0.22	6.1	1
Isoform GluR6-2 of Glutamate receptor	NP_034478.1	0.22	1.5	1
BTB (POZ) domain containing 12	NP_803423.2	0.22	0.7	1
calcium and integrin binding 1 (calmyrin)(blast)	NP_036000.1	0.22	4.2	1
laminin,beta 2(blast)	NP_032509.2	0.22	1.7	1
Isoform 3 of Kelch-like protein 26	NP_742049.1	0.21	2.7	1
gem (nuclear organelle) associated protein 4 (blast)	NP_796341.1	0.21	1.2	1
ATP-dependent RNA helicase DDX41	NP_598820.1	0.21	3.7	1

(+) Bone

Matrix Metalloproteinase 9	NM_013599	0.68	13	9
Myosin-4	NP_034988.2	1	3	5.15
Myosin-1	NP_001074688.1	1	3	5.15
mannosidase 2	O54782	0.86	1	1.5
Nuclear RNA export factor 7	NP_570958.1	0.73	3	1.55
Zfp473 protein	NP_848849.2	0.65	13	7.3
high density lipoprotein binding protein (blast)	Q3U4Z7	0.62	1	1.09
Isoform 2 of Teneurin-3	NP_035986.2	0.54	3	1.87
Fat4	Q2PZL6	0.47	1	0.83
GDP-mannose 4,6 dehydratase	Q8K0C9	0.42	2	1.24
Olfactory receptor 681	NP_997440.1	0.38	2	1.06
ATP-binding cassette transporter sub-family A member 9 (blast)	NP_671753.1	0.3	1	0.53
tubulin, beta 4(blast)	NP_033477.2	0.24	1	0.41
p47 protein (blast)	XP_977730.1	0.22	3	1.02
Isoform 1 of von Willebrand factor precursor	NP_073725.2	0.21	5	0.85
mannose-6-phosphate receptor binding protein 1	NP_080112.1	0.2	3	0.49
6-phosphogluconate dehydrogenase(blast)	NP_001074743.1	1	10.2	10
Phosphoglycerate kinase 1	NP_032854.2	1	18.3	5
Vimentin	NP_035831.2	1	5.4	4
isocitrate dehydrogenase 1 (NADP+), soluble (blast)	NP_034627.2	1	11.4	3
gelsolin [Mus musculus](blast)	NP_666232.2	1	17.5	16
actin-related protein 2 [Mus musculus](blast)	NP_082789.1	1	19.1	12
Isoform 1 of Rab GDP dissociation inhibitor beta	NP_005334.1	0.98	2.7	1
Cathepsin D precursor	NP_035616.1	0.97	7.8	1
Citrate synthase, mitochondrial precursor	NP_080720.1	0.86	2.4	3
protein-tyrosine kinase fyn [Mus musculus] (blast)	NP_032080.1	0.61	8	9
C-Src kinase	NM_001025395	0.85	13	18
SMC5 protein	NP_722503.1	0.2	1.2	1
Vacuolar ATP synthase catalytic subunit A	XP_898621.1	1	10.8	23
71 kDa protein,Heat shock cognate 71 kDa protein	P97805	0.83	2.7	1
Protein FAM3D precursor	NP_001034283.1	0.68	2.4	10
Isoform 2 of Apoptosis-inducing factor-like	NP_035986.2	0.45	0.8	1
Cathepsin K	NP_031828	0.6	12.3	16
6-phosphogluconate dehydrogenase,	NP_001074743.1	1	16.8	12

Vimentin	NP_035831.2	1	13.3	7
vacuolar H+ATPase B2 [Mus musculus](blast)	NP_031535.2	1	4.8	4
Isoform 1 of Rab GDP dissociation inhibitor beta	NP_005334.1	1	7.6	2
Pyruvate kinase isozyme M2	P52480	1	6.6	2
actin-related protein 2 (blast)	NP_082789.1	1	22.1	35
Creatine kinase B-type	Q04447	1	32.5	81
enolase 1	NP_075608.1	1	16.2	10
Heterogeneous nuclear ribonucleoprotein H1	NP_067485.1	1	7.6	2
isocitrate dehydrogenase 1 (NADP+), soluble(blast)	NP_034627.2	0.98	4.1	2
Elongation factor 1-gamma,49 kDa protein	Q4FZK2	0.98	4	1
Citrate synthase, mitochondrial precursor	NP_080720.1	0.93	2.4	6
Phosphoglycerate kinase 1	NP_032854.2	0.93	8.3	1
Nucleolin	NP_035010.3	0.82	3	1
Sodium\potassium-transporting ATPase subunit beta-3	P97370	0.79	6.1	2
Isoform 2 of Teneurin-3	NP_035986.2	0.76	0.8	11
26S protease regulatory subunit S10B	P62333	0.76	3.9	1
Isoform C of Lamin-A\C	NP_001002011.1	0.72	1.7	1
Ubiquinol-cytochrome-c reductase complex core protein I	Q9CZ13	0.65	4.4	1
Ubiquitin-protein ligase E3 component N-recognin-1	NP_033487.1	0.54	0.7	1
Cation-dependent mannose-6-phosphate receptor precursor	P24668	0.52	6.5	1
Transient receptor potential cation channel subfamily M	NP_612174.1	0.5	0.7	1
S1 protein C2,Heterogeneous nuclear ribonucleoprotein A\B	NP_001041526.1	0.49	4.9	1
Myosin IIIB2,myosin IIIB	NP_796350.2	0.4	1	1
protein-tyrosine kinase fyn [Mus musculus](blast)	NP_032080.1	0.35	1.9	1
vesicle-associated calmodulin-binding protein (blast)	NP_663596.1	0.31	5.1	25
DVL-binding protein DAPLE	NP_080957.2	0.29	0.7	2
Isoform 1 of Discs large homolog	NP_031888.2	0.27	1.7	1
ATPase, H+ transporting, V1 subunit A, isoform 1	NP_598587.2	1	3.2	8
Plastin-2 or L-Plastin	NP_032905.2	1	12.3	13
Heat shock cognate 71 kDa protein	XP_898621.1	1	9.6	7
Myosin-4	NP_034988.2	1	2.3	9
cortactin	NP_031829.2	1	19.2	31
Isoform 2 of Teneurin-3	NP_035986.2	0.24	0.8	2
Stress-70 protein, mitochondrial precursor	XP_998290.1	0.67	2.8	1

Table S2

Gene name	Forward	Reverse
Arp3	5'- ctttgaaacccatcatcac -3'	5'- ttccattgatcttcccaatac -3'
Gelsolin	5'- cttctgctaagcggtacatc -3'	5'- agatggacaaccctcaaag -3'
Integrin αv	5'- cctgaggtgcttcttaagtg -3'	5'- ggcgaagtaaatgtaacctg -3'
Integrin β3	5'- tcctctatgtggtggaag -3'	5'- tctttatacagcgggttg -3'
PTP-PEST	5'- agcattgcaggttatcagag -3'	5'- tccaaggcacttactgaatc -3'
Pyk2	5'- tgatacagaggggacagag -3'	5'- catccaggtcaaactcac -3'
Rho	5'- gcctctgtatctgcaaagag -3'	5'- catcccattcttttgctaag -3'
Rho GAP	5'- agcagcatgactgttgtg -3'	5'- gctgcttcaactctattg -3'
Rho kinase	5'- cagcttcttcacctgtcttc -3'	5'- tttcagacagaaaggcactc -3'
WASP	5'- ctgccatctagattctgctc -3'	5'- gggaaagaaacccaaactac -3'
Actin	5'- tcttccgccttaatacttc -3'	5'- tagtcaagttcgaccgtc -3'
18S	5'- *acgaggaattcccagtaag -3'*	5'- *gagaccaaagccttcatac -3'*
GAPDH	5'- *gaggaccaggttgtctcctg* -3'	5'- *atgtaggccatgaggtccac* -3'
c-Src	5'- cttctctctgcctcagtgtc -3'	5'- tctgggatagagtagggatg -3'
Plastin-2	5'- taccgccatagcatcttc -3'	5'- ggaggcagatggacaaac -3'
Cortactin	5'- ggcttccttgagcaactgtc-3'	5'- gcaaggattctgcaggaaag -3'

Figure S4

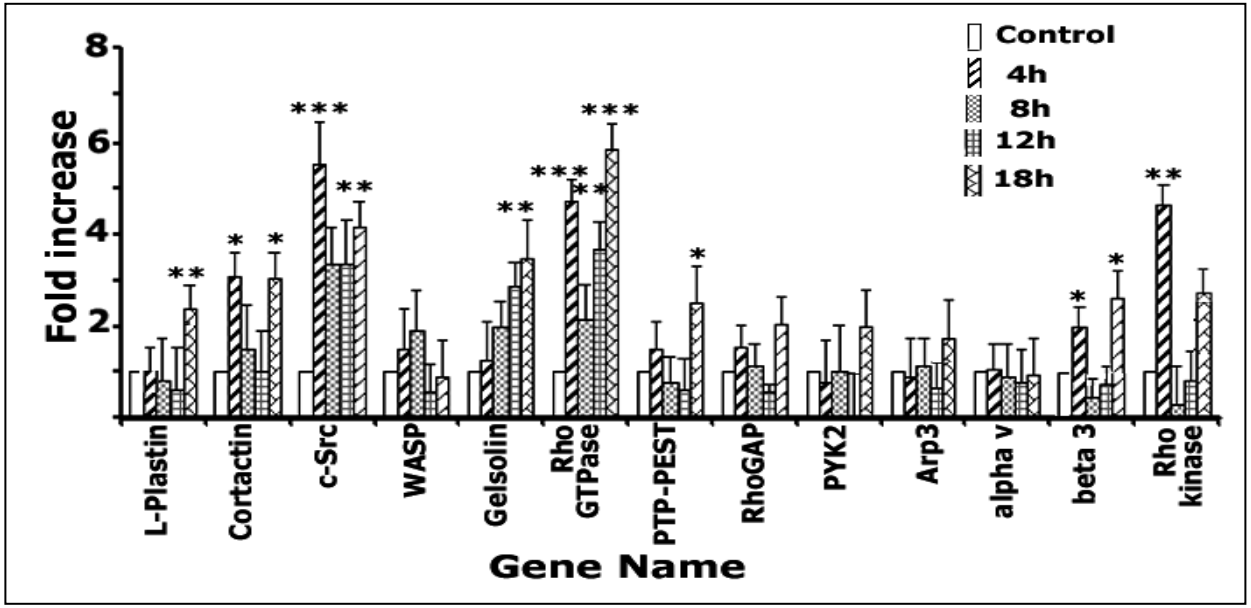

Figure S5